1    **Hippo signaling restricts cells in the second heart field that differentiate**

2    **into Islet-1-positive atrial cardiomyocytes**

3

4    Hajime Fukui[1], Takahiro Miyazaki[1], Hiroyuki Ishikawa[1], Hiroyuki Nakajima[1], and

5    Naoki Mochizuki[1,2]*

6

7    [1]Department of Cell Biology, National Cerebral and Cardiovascular Center

8     Research Institute, Fujishirodai 5-7-1, Suita, Osaka 565-8565, Japan

9    [2]AMED-CREST

10

11

12    ***For Correspondence**: Naoki Mochizuki: nmochizu@ri.ncvc.go.jp

13    Department of Cell Biology, National Cerebral and Cardiovascular Center

14    Research Institute, Fujishirodai 5-7-1, Suita, Osaka 565-8565, Japan

15    Phone: +81-6-6833-5012; FAX: +81-6-6835-5461

16

17

18 **Abstract**

19 Cardiac precursor cells (CPCs) in the first heart field (FHF) and the second

20 heart field (SHF) present at both arterial and venous poles assemble to form a

21 cardiac tube in zebrafish. Hippo kinase cascade is essential for proper heart

22 formation; however, it remains elusive how Hippo signal contributes to early

23 cardiac fate determination. We here demonstrate that mutants of *large tumor*

24 *suppressor kinase 1/2* (*lats1/2*) exhibited an increase in a SHF marker, Islet1

25 (Isl1)-positive and *hand2* promoter-activated venous pole atrial cardiomyocytes

26 (CMs) and that those showed expansion of the domain between between the

27 anterior and the posterior lateral plate mesoderm. Consistently, TEAD-

28 dependent transcription was activated in caudal region of the left ALPM cells

29 that gave rise to the venous pole atrial CMs. Yap1/Wwtr1-promoted *bmp2b*

30 expression was essential for Smad-regulated *hand2* expression in the left

31 ALPM, indicating that Hippo signaling restricts the SHF cells originating from the

32 left ALPM that move toward the venous pole.

33

eLIFE -Research article (Full Submission)-
Fukui et al.
30-05-2017-RA-eLife-29106

## Introduction

Heart forms mainly according to the assembly of cardiomyocytes (CMs) and

blood vessel-constituting cells that originate from anterior lateral plate

mesoderm (ALPM). The ALPM can be distinguished from the posterior lateral

plate mesoderm (PLPM) at the 6-8 somite stage (ss) (Waxman et al., 2008).

The embryonic heart field is specified during formation of ALPM (Fishman and

Chien, 1997). Bilaterally located cells that finally differentiate into heart field

cells migrate medially and fuse at the midline to form the cardiac tube (Staudt

and Stainier, 2012). Several signaling pathways exert roles to restrict the heart

field potency at the both rostral and caudal boundaries of the ALPM. The

retinoic acid (RA) signaling determines the forelimb field by restricting the

posterior end of heart field (Waxman et al., 2008). Tal1 and Etv2 are

transcriptional factors for vascular and hematopoietic lineage specification,

respectively, and repress cardiac specification in rostral ALPM region

(Schoenebeck et al., 2007). While the heart field is defined by restriction of the

other organ fields in the ALPM (Fishman and Chien, 1997), it remains unclear

which signals regulate the differentiation of ALPM into heart field and the other

fields.

In vertebrates, the first heart field (FHF)-derived CMs and the second heart

field (SHF)-derived CMs contribute to the initial tube formation and to the

accretion of CMs at the arterial and venous poles, respectively (Kelly et al.,

2014). These cells in the FHF and SHF are thus cardiac precursor cells (CPCs).

During heart development in chick and mouse embryos, the progenitors of the

venous pole are located most laterally and caudally in the ALPM (Abu-Issa and

eLIFE -Research article (Full Submission)-
Fukui et al.
30-05-2017-RA-eLife-29106

58  Kirby, 2008; Galli et al., 2008). While mammalian SHF-derived CMs have been

59  characterized extensively using lineage-tracing (Cai et al., 2003; Galli et al.,

60  2008; Abu-Issa and Kirby, 2008), specification and expansion of zebrafish SHF-

61  derived cells remains unclear. Successive phases of CM differentiation are

62  conserved among vertebrates during the development of myocardium (Staudt

63  and Stainier, 2012), although zebrafish heart consists of one atrium and one

64  ventricle in contrast to four-chambered heart in mammals.

65      In zebrafish, a LIM homeodomain transcription factor, Islet-1 (Isl1)-positive

66  SHF cells give rise to CMs in the venous pole and consequent inflow tract (IFT)

67  CMs of the atrium, whereas Isl2b and latent TGFβ binding protein 3 (Ltbp3)-

68  positive SHF cells become CMs only at the arterial pole and subsequently

69  contribute to the formation of outflow tract (OFT) of the ventricle (de Pater et al.,

70  2009; Zhou et al., 2011; Witzel et al., 2017). While the number of CMs in the

71  venous pole in *isl1* mutants is decreased, that at the arterial poles remains

72  unchanged (de Pater et al., 2009). Ltbp3-positive SHF cells express

73  transcription factors, Nkx2.5 and Mef2c that are also expressed in the FHF

74  (Guner-Ataman et al., 2013; Hinits et al., 2012). Another transcription factor,

75  Hand2, a basic helix-loop-helix transcription factor, is involved in the arterial

76  pole formation by the CPC in the SHF (Schindler et al., 2014). While the

77  essential and potential roles of these transcription factors during cardiogenesis

78  have been reported (Guner-Ataman et al., 2013; Hinits et al., 2012; Schindler et

79  al., 2014), it remains elusive how the expression of these transcription factors is

80  regulated.

81      Hippo signaling pathway defines the number of cells in tissue/organ

eLIFE -Research article (Full Submission)-
Fukui et al.
30-05-2017-RA-eLife-29106

82  including heart (Zhou et al., 2015). Mammalian Ste20-like serine/threonine

83  kinase 1 and 2 (Mst1/2, mammalian orthologs of fruit fly, Hippo) phosphorylate

84  Large tumor suppressor kinase 1 and 2 (Lats1/2). Phosphorylated Lats1/2

85  induce nuclear export of Yes-associated protein 1 (Yap1) / WW domain

86  containing transcription regulator 1 (Wwtr1, also known as Taz), thereby

87  inhibiting Yap1/Wwtr1-TEA domain (TEAD) transcription factor complex-

88  dependent expression of genes essential for cell specification, proliferation,

89  survival, and differentiation (Zhao et al., 2008; Nishioka et al., 2009). Hippo

90  signaling has been implicated in heart formation as well as regeneration after

91  myocardial injury (Lin et al., 2014; von Gise et al., 2012; Xin et al., 2013).

92  Nuclear Yap1 drives the proliferation of CM in adult and fetal mouse heart. Mice

93  depleted of *Lats2*, *Salvador* (*Salv*), or *Mst1/2* using CM-specific Cre drivers

94  exhibit a hypertrophic growth owing to an increase of CMs (Zhou et al., 2015).

95  *Yap1* and *Wwtr1* double-null mutant mice are embryonic lethal before the

96  blastula stage (Nishioka et al., 2009), suggesting the essential role for

97  Yap1/Wwtr1 in early cardiovascular development, although it is unclear whether

98  Yap1/Wwtr1 function in the FHF/SHF-dependent cardiac development.

99       In this study, we demonstrate that Lats1/2-Yap1/Wwtr1-regulated hippo

100  signaling determines the fate of cells between ALPM and PLPM that influences

101  the number of both *hand2* and *isl1* promoter-activated SHF cells. Moreover, we

102  reveal that Yap1/Wwtr1 promote *bone morphogenetic protein-2b* (*bmp2b*)

103  expression in the ALPM required for accretion in the venous pole and

104  subsequent inflow tract (IFT) atrial CMs development.

105

eLIFE -Research article (Full Submission)-
Fukui et al.
30-05-2017-RA-eLife-29106

**Results**

**Lats1/2 are involved in atrial CMs development**

106

107

108    To examine whether Yap1/Wwtr1-dependent transcription determines the CMs

109    number during early cardiogenesis, we developed *lats1* and *lats2* knockout

110    (KO) fish using transcription activator-like effector nuclease (TALEN)

111    techniques. The fish with *lats1$^{ncv107}$* and *lats2$^{ncv108}$* allele lacked 10 bp at Exon 2

112    and 16 bp at Exon 3, respectively, and had premature stop codons due to frame

113    shifts (Figure 1—Figure supplement 1A). Either *lats1$^{ncv107}$* KO fish or *lats2$^{ncv108}$*

114    KO fish was viable with no apparent defect (data not shown). However, almost

115    all of the *lats1$^{ncv107}$lats2$^{ncv108}$* double KO (*lats1/2* DKO) larvae died before 15

116    days post-fertilization (dpf) (Figure 1—Figure supplement 1B).

117        We examined the effect of Lats1/2 depletion on heart development by

118    counting CM numbers in atrium and ventricle in *Tg(myosin heavy chain 6*

119    *[myh6]:Nls-tdEosFP);Tg(myl7:Nls-mCherry)* larvae with *lats1/2* mutant alleles

120    that expressed Nls-tagged tandem EOS fluorescent protein under the control of

121    atrium-specific *myh6* promoter and Nls-mCherry under the control of *myl7*

122    promoter (Figure 1A). The number of atrial CMs but not ventricular CMs was

123    significantly increased in *lats1$^{wt/\ ncv107}$lats2$^{ncv108}$* embryos and

124    *lats1$^{ncv107}$lats2$^{ncv108}$* embryos at 74 hours post-fertilization (hpf) (Figure 1B, C

125    and Figure 1—source data 1).

126        To examine whether Yap1/Wwtr1-dependent transcription is activated during

127    embryogenesis and in CMs, we used two Tead reporter Tg lines: one expressed

128    human TEAD2 lacking amino-terminus (1–113 aa) fused with GAL4 DNA-

129    binding domain under the control of *eukaryotic translation elongation factor 1*

6

eLIFE -Research article (Full Submission)-
Fukui et al.
30-05-2017-RA-eLife-29106

130    *alpha 1, like 1* (*eef1a1l1*) promoter, *Tg(eef1a1l1:galdb-hTEAD2ΔN-2A-*

131    *mCherry)* ; the other expressed that under the control of CM-specific *myosin*

132    *light polypeptide 7* (*myl7*) promoter, *Tg(myl7:galdb-hTEAD2ΔN-2A-mCherry).* In

133    these Tg fish crossed with *Tg(uas:GFP)*, when Yap1 or Wwtr1 entered the

134    nuclei, GFP expression was promoted according to the Gal4-UAS system

135    (Fukui et al., 2014). Hereafter, we named the former, general Tead reporter, and

136    the latter, CM Tead reporter, respectively. GFP-expressing cells reflected the

137    nuclear translocation of Yap1 and/or Wwtr1. Yap1/Wwtr1-dependent

138    transcriptional activation defined by increased GFP expression was found in

139    *lats1/2* DKO embryos and *lats1/2* morphants (Figure 1—Figure supplement 2A),

140    suggesting that these KO fish allow us to examine when and where

141    Yap1/Wwtr1-Tead complex-dependent transcription was activated. The CPCs in

142    the venous pole become the IFT atrial CMs (de Pater et al., 2009). We

143    confirmed Yap1/Wwtr1-dependent transcription in IFT atrial CMs by the CM

144    Tead reporter fish embryos at 74 hpf (Figure 1—Figure supplement 2B).

145    At 24 hpf, GFP expression was observed in the *myl7* promoter-activated

146    CMs of the venous pole but not the other area of general Tead reporter crossed

147    with *Tg(myl7:Nuclear localization signal [Nls]-tagged mCherry)* fish (Figure 1—

148    Figure supplement 2C). In this Tg fish embryos, mCherry expression driven by

149    *eef1a1l1* and 2A peptide was subtle compared to that driven by *myl7* promoter.

150    These data suggest that Lats1/2 restrict the Yap1/wwtr1-Tead signal-dependent

151    increase in atrial CM number during early cardiac development.

152

153    **Lats1/2 determine the number of CMs derived from the *hand2* promoter-**

7

eLIFE -Research article (Full Submission)-
Fukui et al.
30-05-2017-RA-eLife-29106

154 **activated CMs**

155 We assumed that an increase in atrial CMs might be ascribed to an increase in

156 CPCs in the SHF, because Yap1/Wwtr1-dependent transcription was observed

157 in the venous pole of heart tube and the IFT CMs of atrium (Figure 1—Figure

158 supplement 2B, C). Firstly, we examined the effect of nuclear Yap1/Wwtr1 on

159 early cardiogenesis by investigating the expression of transcription factors,

160 *nkx2.5*, *hand2*, and *gata4,* essential for early CPC differentiation (Schoenebeck

161 et al., 2007). Among these transcription factors, *hand2* mRNA expression was

162 significantly up-regulated in the *lats1/2* morphants (Figure 2A and Figure 2—

163 source data 1). The expression of *nkx2.5* and *gata4* mRNAs was unaffected by

164 the depletion of Lats1/2 (Figure 2A and Figure 2—source data 1). The whole

165 mount *in situ* hybridization (WISH) analyses revealed that *hand2* expression

166 was increased in the domain that was supposed to give rise to the heart in

167 *lats1^{wt/ ncv107}lats2^{ncv108}* embryos, *lats1/2* DKO embryos and *lats1/2* morphants at

168 22 hpf (Figure 2B and Figure 2—Figure supplement 1A). These data suggest

169 that Lats1/2 might determine the number of atrial CMs through the control of

170 *hand2* expression.

171 Overexpression of Hand2 increases the number of SHF-derived CMs but

172 not FHF-derived CMs in zebrafish (Schindler et al., 2014). To investigate the

173 relevance of *hand2* expression to CM number in the atrium, we tried to count

174 the number of *hand2*-positive CMs at early time point using Tg fish expressing

175 GFP under the control of *hand2* BAC promoter; *TgBAC(hand2:GFP) (Yin et al.,*

176 *2010)*. We crossed this Tg fish with *Tg(myl7:Nls-mCherry)* to count the number

177 of both *hand2* and *myl7* promoter-activated CMs at 26 hpf. Both promoter-

8

178 activated CMs were localized at the anterior side of growing heart tube

179 corresponding to the venous pole (Figure 2C). In the *lats1/2* DKO embryos, the

180 number of both promoter-activated CMs was significantly increased in the

181 venous pole (Figure 2C, D and Figure 2—source data 1). Consistent with these

182 results, the both promoter-activated cells were increased in the venous pole in

183 the *lats1/2* morphants (Figure 2—Figure supplement 1B). To examine the

184 function of Yap1/Wwtr1, we developed double KO of *yap1* (Figure 2—Figure

185 supplement 2A) and *wwtr1* (Nakajima et al., 2017). In the *yap1* and *wwtr1* DKO

186 embryos, *hand2* promoter-activated cells were greatly reduced. Those double

187 mutant embryos exhibited cardia bifida (Figure 2—Figure supplement 2B).

188 These results suggest that Lats1/2 are involved in the formation of *hand2*

189 promoter-activated cells present in the venous pole cells that give rise to the IFT

190 atrial CMs.

191

192 **hand2 promoter-activated cells in the caudal end of the left ALPM migrate**

193 **toward venous pole of heart tube**

194 The progenitors of the venous pole are located most caudally in the ALPM in

195 the mammalian heart (Abu-Issa and Kirby, 2008; Galli et al., 2008). To

196 investigate how *hand2* promoter-activated cells contribute the venous pole cells

197 that differentiate into CPCs, we time-lapse imaged them from 14 hpf to 26 hpf.

198 Certain number of cells in the caudal side of the left ALPM migrated toward the

199 venous pole, whereas those of the right ALPM migrate into the arterial pole

200 (Figure 3A, B, and Video 1). The cell tracking analyses demonstrated that both

201 former and latter cells moved toward the region where the cardiac disk

eLIFE -Research article (Full Submission)-
Fukui et al.
30-05-2017-RA-eLife-29106

202 developed at 20 hpf and subsequently became venous pole and arterial pole,

203 respectively (Figure 3A-C). These results indicate that *hand2* promoter-

204 activated cells in the caudal region of the left ALPM differentiate into the venous

205 pole cells. This directional migration of the *hand2* promoter-activated cells in the

206 caudal region of the ALPM cells was further confirmed by the embryos with situs

207 inversus. The *polycystin-2* (*pkd2)* morphant causes the randomization of left-

208 right patterning which often results in situs inversus (Bisgrove et al., 2005). The

209 caudal region of right ALPM moved toward the venous pole cells of the heart of

210 the embryos with situs inversus. (Figure 3—Figure supplement 1 and Video 2).

211 Collectively, the directional migration of the cells in the caudal region of the

212 ALPM cells toward the venous pole might be predetermined by uncertain

213 signaling.

214　　We next tracked Tead transcription-activated cells using general Tead

215 reporter fish embryos. At 14 hpf, the Tead reporter-activated cells were located

216 in the caudal region of the left ALPM (Figure 3D). Subsequently, these cells

217 moved toward the venous pole similarly to the *hand2* promoter-activated cells

218 (Figure 3D, E, and Video 3). We further found that the migration speed of the

219 cells initially located in the caudal region of the left ALPM (the pink line of Figure

220 3F and Figure 3—source data 1) migrating toward the venous pole was very

221 similar to that of the Tead reporter-activated cells (from 21 hpf to 24 hpf) (the

222 green line of Figure 3F and Figure 3—source data 1), suggesting that those

223 cells are likely to be the same cells and that Tead-activated cells become the

224 venous pole cells. Furthermore, these data imply that the number of the cells

225 might be decided by Hippo signaling.

eLIFE -Research article (Full Submission)-
Fukui et al.
30-05-2017-RA-eLife-29106

226

**Lats1/2 determine the number of IFT CMs derived from the Isl1-positive**

**SHF cells**

We, next, investigated whether both *hand2* and *myl7* promoter-activated cells

are the SHF-derived cells that add to the growing heart tube in the venous pole.

We used Isl1 as a SHF marker, because Isl1 plays an essential role for the

development of CPCs in the SHF and forms complex with key regulatory

molecules for SHF development, such as Hand2 (Cai et al., 2003; Caputo et al.,

2015). We found that in the *lats1/2* DKO embryos, Isl1-positive SHF cells were

increased and overlapped both *hand2* and *myl7* promoter-activated CMs in the

very left-rostral end of heart tube (Figure 4A, brackets). Consistently, the

number of both promoter-activated Isl1-positive CMs in the *lats1/2* morphants

was increased (Figure 4—Figure supplement 1A). Furthermore, general Tead

reporter-activated cells were positive for Isl1 in the venous pole and were

increased by the depletion of Lats1/2 (Figure 4—Figure supplement 1B, arrows

and Figure 4—Figure supplement 1C).

To characterize *isl1* promoter-activated SHF cells during early stage and to

examine whether those cells become CMs of the IFT, we generated Tg fish

expressing GFP under the control of *isl1* BAC promoter; *TgBAC(isl1:GFP). isl1*

promoter-activated cells were found in the IFT of atrium at 4 dpf (Figure 4B, C

and Figure 4—source data 1). While *isl1* promoter-activated cells were

observed in the endocardium and epicardium at 96 hpf (Figure 4—Figure

supplement 1D, arrows and arrowheads), those cells were found in neither

arterial pole, OFT, nor ventricular myocardium until 4 dpf (Figure 4B, C and

11

eLIFE -Research article (Full Submission)-
Fukui et al.
30-05-2017-RA-eLife-29106

250  Figure 4—source data 1). The number of *isl1* promoter-activated cells in the

251  venous pole was significantly increased in either *lats1^{wt/ncv107}lats2^{ncv108}* embryos

252  or *lats1/2* DKO embryos at 26 hpf (Figure 4D, E and Figure 4—source data 1).

253  Consistent with this, the *isl1* promoter-activated SHF cells were significantly

254  increased in the venous pole in the *lats1/2* morphants (Figure 4F, Figure 4—

255  Figure supplement 1E and Figure 4—source data 1). Ajuba, a LIM-domain

256  family protein, restricts Isl1-positive SHF cells by binding to Isl1 (Witzel et al.,

257  2012). The number of *isl1* promoter-activated SHF cells were increased in the

258  *ajuba* morphants (Figure 4F, Figure 4—Figure supplement 1E and Figure 4—

259  source data 1). We also found that in the embryos expressing a mCherry-

260  tagged dominant-negative form of Yap1/Wwtr1-Tead-dependent transcription

261  (ytip-mCherry) (Fukui et al., 2014), the *isl1* promoter-activated SHF cells were

262  significantly decreased in the venous pole (Figure 4F, Figure 4—Figure

263  supplement 1E and Figure 4—source data 1). Therefore, we confirmed that

264  Lats1/2-mediated hippo signaling is involved in the accretion of SHF-derived

265  CPCs in the venous pole.

266

267  **Yap1/Wwtr1 promote the differentiation of SHF cells from the caudal end**

268  **of ALPM**

269  Tead reporter activation in the cells of ALPM as shown in Figure 3F prompted

270  us to ask whether Lats1/2-Yap1/Wwtr1 signal is involved in either or both

271  proliferation and/or specification of those cells into the Isl1-positive SHF cells

272  from the ALPM. To investigate whether the increase in the number of SHF cells

273  in *lats1/2* DKO embryos and *lats1/2* morphants is ascribed to the proliferation of

eLIFE -Research article (Full Submission)-
Fukui et al.
30-05-2017-RA-eLife-29106

274    the SHF cells that have differentiated from the ALPM, we examined proliferation

275    of *isl1* promoter-activated cells by the EdU incorporation assay. The number of

276    *isl1* promoter-activated EdU-positive CM of the *lats1/2* morphants was

277    comparable to that of the control (Figure 5A, B). There was no difference of the

278    number of EdU-positive blood cells and endocardial cells among the two groups

279    (data not shown). Furthermore, the timing of EdU incorporation did not affect

280    the results of the proliferation analyses (Figure 5B), suggesting that the

281    increased number of *isl1*-positive SHF cells in the depletion of Lats1/2 is not

282    caused by the cell proliferation after the differentiation of SHF cells from the

283    ALPM.

284         We, therefore, asked whether Lats1/2 restrict SHF cell specification from

285    the ALPM. To test this hypothesis, we examined the expression of both ALPM

286    and PLPM genes: *gata4* as a marker for multipotent myocardial-endothelial-

287    myeloid progenitor of ALPM; *nkx2.5* as a marker for ventricular heart field; *tal1*

288    as a marker for hematopoietic cell progenitor; and *hand2* as a marker for both

289    heart field and PLPM at 10 ss (Figure 5C). There was a gap of *hand2*

290    expression between ALPM and PLPM in the WT embryos but the gap length

291    was significantly shorten in either *lats1$^{wt/ncv107}$lats2$^{ncv108}$* embryos or *lats1/2* DKO

292    embryos as well as the *lats1/2* morphants (Figure 5D, E, Figure 5—Figure

293    supplement 1A and Figure 5—source data 1). In clear contrast, *tal1* expression

294    was decreased in the rostral end of PLPM in the *lats1/2* DKO embryos and

295    *lats1/2* morphants (Figure 5F and Figure 5—Figure supplement 1B). Although

296    *hand2* expression was decreased in the both ALPM and PLPM in the

297    *yap1/wwtr1* DKO embryos, the expression of *tal1* was unaffected (Figure 5D,

eLIFE -Research article (Full Submission)-
Fukui et al.
30-05-2017-RA-eLife-29106

298    F). The expression of *gata4* and *nkx2.5* was unaffected in the both *lats1/2* DKO

299    embryos and *lats1/2* morphants (Figure 5G, and Figure 5—Figure supplement

300    1C), these results were consistent with the results of qRT-PCR using embryos

301    at 24 hpf (Figure 2A). We further examined other genes regulating heart field;

302    *etv2* as a marker for blood-vessel progenitor (Schoenebeck et al., 2007) and

303    *hoxb5b* as *a* regulatory molecule of RA signaling in the forelimb field (Waxman

304    et al., 2008). The expression of both *etv2* and *hoxb5b* was comparable between

305    the control and the *lats1/2* morphants (Figure 5—Figure supplement 1C).

306    Collectively, these results suggest that Lats1/2 negatively regulates

307    Yap1/Wwtr1-dependent differentiation of LPM to the SHF in the boundary

308    between ALPM and PLPM.

309

310    **Yap1/Wwtr1 drive Bmp-Smad signaling essential for SHF formation**

311    Bone morphogenetic proteins (Bmps)-mediated signal affects the various

312    context of heart development via Smad phosphorylation-dependent

313    transcriptional activation. Bmp-Smads signaling is known to be essential for

314    SHF formation, FHF-derived CM development, endocardium development, and

315    epicardium development (Prall et al., 2007; Schlueter et al., 2006; Tirosh-Finkel

316    et al., 2010; Yang et al., 2006). Yap1 promotes *Bmp2b* expression in the

317    neocortical astrocyte differentiation (Huang et al., 2016). In the zebrafish

318    embryos, *bmp2b*, but not *bmp4*, is expressed in the LPM (Chung et al., 2008).

319    We hypothesized that Yap1/Wwtr1 are involved in *bmp2b*-dependent signal

320    during early cardiogenesis. To investigate whether Bmp-Smad signaling is

321    activated in the ALPM, we examined the Bmp-dependent transcription using Tg

eLIFE -Research article (Full Submission)-
Fukui et al.
30-05-2017-RA-eLife-29106

322  fish in which Bmp responsive element (BRE) drives GFP expression;

323  *Tg(BRE:GFP)* (Collery and Link, 2011). At 14 hpf, BRE-positive cells were found

324  in the ALPM (Figure 6A). BRE-positive cells in the caudal end of ALPM moved

325  toward the venous pole (Video 4). At 10 ss, *bmp2b* expression was increased in

326  the ALPM in the *lats1/2* DKO embryos and was decreased in the *yap1/wwtr1*

327  DKO embryos (Figure 6B). Consistently, *bmp2b* mRNAs were increased in the

328  *lats1/2* morphants at 10 ss (Figure 6—Figure supplement 1A). Although we

329  could not detect *bmp4* in the ALPM in the early ss (data not shown), *bmp4*

330  mRNAs were increased in the venous pole of the *lats1/2* morphants at 26 hpf

331  (Figure 6—Figure supplement 1B).

332      The zebrafish bmp2b is essential for dorsoventral patterning before the

333  formation of heart (Kishimoto et al., 1997). To examine the role of bmp2b on the

334  ALPM cells that become the *hand2* promoter-activated cells in the venous pole,

335  we applied the heat shock-dependent overexpression of bmp2b.

336  Overexpression of bmp2b led to an increase in the number of both *hand2* and

337  *myl7* promoter-activated cells in the venous pole of the embryos at 26 hpf

338  (Figure 6C, D and Figure 6—source data 1). These data suggest that bmp2b-

339  dependent signal can promote *hand2* expression when ALPM cells become the

340  cells in the venous pole.

341      The number of Bmp signal-activated cells marked by GFP in the venous

342  pole was increased in either $lats1^{wt/ncv107}lats2^{ncv108}$ embryos or *lats1/2* DKO

343  embryos as well as the *lats1/2* morphants at 24 hpf (Figure 6E, F, Figure 6—

344  Figure supplement 2A and Figure 6—source data 1). Because Bmps induce

345  phosphorylation of Smad1/5/9 (Smad9 is also known as Smad8) (Heldin et al.,

eLIFE -Research article (Full Submission)-
Fukui et al.
30-05-2017-RA-eLife-29106

346    1997), we examined phosphorylation of Smad1/5/9 in the venous pole at 26 hpf.

347    The number of phosphorylated Smad1/5/9-positive and *hand2* promoter-

348    activated cells was increased in the venous pole of the *lats1/2* morphants at 26

349    hpf (Figure 6—Figure supplement 2B). These results suggest that Yap1/Wwtr1

350    promote *bmp2b* expression and induce the subsequent signaling and that

351    Lats1/2 restrict this Yap1/Wwtr1-dependent signaling to form the proper venous

352    pole.

353         To investigate whether Bmp-Smad signal functions to promote *hand2*

354    expression in a cell-autonomous manner, we performed mosaic analysis.

355    Smad7, an inhibitory-Smad, blocks the Bmp-Smad signal by interacting with

356    activated Bmp type I receptors and thereby preventing the activation of

357    receptor-regulated Smads (Souchelnytskyi et al., 1998). The number of *isl1*

358    promoter-activated cells was decreased in the *TgBAC(isl1:GFP);Tg(myl7:Nls-*

359    *mCherry)* embryos injected with *smad7* mRNA at 26 hpf (Figure 6—Figure

360    supplement 2C). We then tested cell autonomous function by injection of *smad7*

361    mRNA in CPC-fated cells (Fukui et al., 2014; Lou et al., 2011) to see *hand2*

362    expression in the caudal region of the left ALPM (Figure 6G). *hand2* promoter-

363    activated GFP signal was suppressed in the cells injected with *smad7* mRNA

364    together *gata5* and *smarcd3b* mRNAs, suggesting the cell-autonomous

365    regulation (Figure 6H).

366         Finally, to confirm the necessity of Bmp-Smad-regulated signal during the

367    SHF formation, we treated *TgBAC(hand2:GFP);Tg(myl7:Nls-mCherry)* embryos

368    with a Bmp inhibitor, DMH1, from 14 hpf to 26 hpf. The efficiency of DMH1 was

369    confirmed by decreased phosphorylation of Smad1/5/9 (Figure 6—Figure

eLIFE -Research article (Full Submission)-
Fukui et al.
30-05-2017-RA-eLife-29106

370 supplement 2B). The expression of Isl1 and the promoter activity of *hand2* were

371 greatly reduced in the embryos treated with DMH1, although the activity of *myl7*

372 promoter monitored by mCherry expression was not affected in the FHF-derived

373 region (Figure 6I). These data suggest that Lats1/2 restrict Yap1/Wwtr1-

374 promoted Bmp2b-dependent signaling cell-autonomously required for both

375 *hand2* and *isl1* promoter-activated SHF formation.

376

eLIFE -Research article (Full Submission)-
Fukui et al.
30-05-2017-RA-eLife-29106

**Discussion**

We here for the first time show that Hippo signal is involved in the determination

of cell fate of LPM cells (Figure 7). While Yap1/Wwtr1-promoted signal

increased the domain of SHF, Lat1/2 restricted it, because Lat1/2 likely to

induce export of Yap1/Wwtr1 from the nucleus. The formation of the boundary

between ALPM and PLPM as well as whole LPM was under the regulation of

Hippo signaling. A cooperative mechanisms by the several signaling pathways

might be involved in the definition of heart field. In the forelimb field, *hoxb5b*

represses the extension of posterior end of heart field that differentiate into atrial

but not ventricular CMs (Waxman et al., 2008). Furthermore, the pronephric

field in the intermediate mesoderm and the angiogenic field in the rostral region

of PLPM are closely associated with restriction of their cell fate in these

boundary (Kimmel et al., 1990; Mudumana et al., 2008). The increased number

of SHF cells in the *lats1/2* DKO embryos may be attributable to the change of

fate determination from *hand2*-negative cells to -positive cells in the boundary

between ALPM and PLPM. Indeed, we found that expression of the marker of

blood-cell progenitor *tal1* was repressed at the rostral region of PLPM in the

*lats1/2* DKO embryos. Although mutants of *lats1/2* exhibited a subtle increase in

the number of Isl1-positive atrial SHF cells with no apparent defect of other

organs, Hippo signaling is involved in the lineage specification of LPM cells.

Zebrafish Isl1-positive SHF cells might correspond to the mammalian

posterior-SHF. In the mouse embryo, the anterior and posterior SHF

differentiate into OFT/right ventricular myocardium and IFT/atrial myocardium,

respectively (Galli et al., 2008; Verzi et al., 2005). The posterior-SHF in the

eLIFE -Research article (Full Submission)-
Fukui et al.
30-05-2017-RA-eLife-29106

401  heart field is located caudally (Galli et al., 2008; Abu-Issa and Kirby, 2008).

402  Pitx2, a member of the paired-like family of homeodomain transcription factors,

403  is expressed in the left LPM for embryonic left-right asymmetry and determines

404  the posterior-SHF formation (Galli et al., 2008). Tead reporter activation

405  occurred in the left side of the caudal zone of ALPM that becomes Isl1-positive

406  venous pole atrial CMs but not ventricular CMs. Caudally-located left and right

407  side of heart fields constituted the venous pole and the arterial pole of cardiac

408  tube, respectively. In addition, mammalian SHF cells have multi-potential to

409  differentiate into endocardium and smooth muscle cells in addition to

410  myocardium (Chen et al., 2009b). By generating BAC transgenic fish, we found

411  that zebrafish *isl1* promoter-activated SHF cells gave rise to atrial myocardium,

412  endocardium, and epicardium, except for ventricular myocardium. Combining

413  with our results and previous reports, the properties of zebrafish Isl1-positive

414  SHF cells are similar to that of the mammalian posterior-SHF cells.

415       Lats1/2-Yap1/Wwtr1-Tead signaling functions upstream of Bmp2b-Smad

416  activation in the ALPM that is necessary for the formation of *hand2* and *isl1*

417  promoter-activated cells. Although the previous reports have shown that Isl1-

418  positive and Mef2-positive cells reside in the venous pole (de Pater et al., 2009;

419  Hinits et al., 2012), the molecular mechanism underlying how these cells give

420  rise to the CPCs in the venous pole has remained unclear. To date, extracellular

421  stimuli TGFβ, FGF, and BMP have been reported to regulate arterial pole

422  formation in zebrafish (de Pater et al., 2009; Hami et al., 2011; Zhou et al.,

423  2011). In addition, transcription factors including Tbx1, Mef2c, and Nkx2.5 are

424  known to control the development of arterial but not venous pole formation

19

eLIFE -Research article (Full Submission)-
Fukui et al.
30-05-2017-RA-eLife-29106

425 (Guner-Ataman et al., 2013; Hinits et al., 2012; Lazic and Scott, 2011). We

426 revealed that Yap1/Wwtr1-Tead dependent transcription is required for *isl1-*

427 promoter activated SHF formation, because the forced expression of

428 Yap1/Wwtr1-Tead binding dominant-negative form (ytip-mCherry) suppressed

429 the formation of *isl1* promoter-activated SHF cells. Furthermore, Bmp reporter

430 activity was observed in the ALPM. By analyzing the Lats1/2 mutants and

431 Yap1/Wwtr1 mutants, we demonstrates that Hippo signal controls *bmp2b*

432 expression in the ALPM. Bmp-Smad inhibition expands *tal1* expression domain

433 to restrict LPM fate (Gupta et al., 2006). In addition, *hand2* expression is

434 diminished in the mutant of *alk3*, a Bmp type I receptor 1a, at 12 ss (de Pater et

435 al., 2012). In our hands, Bmp-Smad inhibition resulted in cell-autonomous

436 suppression of the *hand2* promoter-positive GFP expression at 15 hpf.

437 Therefore, Bmp2b expression positively regulated by Yap1/Wwtr1 balances the

438 cell fate to the heart field and to the blood cells in the boundary between ALPM

439 and PLPM.

440     In summary, we demonstrate that Yap1/Wwtr1-Tead signal promotes

441 Bmp2b expression and activates subsequent Smad signaling in the cells

442 located in the left side of caudally-located ALPM (Figure 7). This signaling

443 determines the Isl1-positive SHF cells in the venous pole that specifically

444 become the IFT atrial CMs lately.

445

eLIFE -Research article (Full Submission)-
Fukui et al.
30-05-2017-RA-eLife-29106

**Materials and methods**

**Zebrafish (*Danio rerio*) strain, transgenic lines and mutant lines**

The experiments using zebrafish were approved by the institutional animal

committee of National Cerebral and Cardiovascular Center and performed

according to the guidelines of the Institute. We used the AB strain as wild-type.

The following zebrafish transgenic lines were used for experiments:

*Tg(eef1a1l1:galdb-hTEAD2ΔN-2A-mCherry)* fish (Fukui et al., 2014),

*Tg(myl7:Nls-mCherry)* fish (Fukui et al., 2014), *TgBAC*(*hand2:GFP*) fish (Yin et

al., 2010), *Tg(BRE:GFP)* fish (Collery and Link, 2011), and *Tg(uas:GFP)* fish

(Asakawa et al., 2008). The *Tg(myl7:galdb-hTEAD2ΔN-2A-mCherry)* fish,

*Tg(myh6:Nls-tdEosFP)* fish, and *TgBAC(isl1:GFP)* fish were generated as

described supplementary experimental procedures. The knockout alleles as

*ncv107* for *lats1*, *ncv108* for *lats2*, and *ncv117* for *yap1* genes were generated

by TALEN techniques as described supplementary experimental procedures.

The *ncv114* allele for *wwtr1* was previously reported (Nakajima et al., 2017).

**Image acquisition by microscopies and image processing**

To clearly obtain the images of embryos, pigmentation of embryos was

suppressed by addition of 1-phenyl-2-thiourea (PTU) (Sigma-Aldrich, St. Loiuis,

MO) into breeding E3 media. Embryos were dechorionated and mounted in 1%

low-melting agarose dissolved in E3 medium. Confocal images were taken with

a FV1200 confocal microscope system (Olympus, Tokyo, Japan) equipped with

water immersion 20x lens (XLUMPlanFL, 1.0 NA, Olympus). Images were

processed with FV10-ASW 4.2 viewer (Olympus). Distance between *hand2*

eLIFE -Research article (Full Submission)-
Fukui et al.
30-05-2017-RA-eLife-29106

470    positive-region of ALPM and PLPM was measured by a DP2-BSW software

471    (Olympus). Cell tracking data containing nuclei positions and instantaneous

472    velocities were analyzed by Imaris8.4.1 software (Bitplane, Zurich, Switzerland).

473

474    **Generation of knockout zebrafish by TALEN**

475    To make knockout zebrafish, we used transcription activator-like effector

476    nuclease (TALEN) Targeter 2.0 (https://tale-nt.cac.cornell.edu) to design TALEN

477    pair that targets *lats1*, *lats2* and *yap1*. The target sequence of TAL-*lats1*, TAL-

478    *lats2, and* TAL-*yap1* were 5'-

479    TCAGCAAATGCTGCAGGAGATccgagagagcctgcgaAACCTCTCCCCGTCCTCC

480    AA-3', 5'-TCTCGAGGAGAGGGTGgtcgaggtggagactCAAAGGGCAAAGACCA-

481    3', and 5'-

482    CCGAACCAGCACAACCctccagccggccaccagaTCGTCCATGTTCGGGG-3',

483    respectively (capital letters were sequences of left [TAL-*lats1*-F*, lats2*-F, and

484    *yap1*-F] and right [TAL-*lats1*-R, *lats2*-R, and *yap1*-R] arms, respectively). These

485    expression plasmids of the TALEN-pair were constructed by pT3TS-

486    GoldyTALEN. TALEN mRNAs were synthesized in vitro by T3 mMessage

487    mMACHINE kit (Thermo Fisher Scientific, Waltham, MA). To induce double

488    strand breaks in the target sequence, both 50 pg of TAL-*lats1-F* / -*lats1-R*

489    mRNAs, TAL-*lats2-F* / -*lats2-R* mRNAs, and TAL-*yap1-F* / -*yap1-R* mRNAs

490    were injected into 1-2-cell stage Tg embryos, respectively. Each injected

491    founder (F0) fish was outcrossed with wild-type fish to obtain F1 progeny from

492    the individual founders. Generation of *wwtr1* knockout zebrafish was previously

493    reported (Nakajima et al., 2017). To analyze TALEN induced mutations,

22

eLIFE -Research article (Full Submission)-
Fukui et al.
30-05-2017-RA-eLife-29106

494    genomic DNA from F1 embryos was lysed by 50 μl of NaOH solution (50 mM) at

495    95°C for 5 min, and added 5 μl of Tris-HCl (pH8.0, 1.0 M) on ice for 10 min.

496    After centrifugation (13,500 rpm, 5 min), PCR reaction was performed by KOD

497    FX Neo DNA polymerase (TOYOBO, Osaka, Japan). The genotyping PCR

498    primers were used for amplification: *lats1* (5'-

499    GGCACTTAACATATGCTTTTACATG-3' and 5'-

500    TTTGCTGCTGTCTGCGGAGCTGTT-3'); *lats2* (5'-

501    AGAGTTTGTGTGAGAGAAAACAGG-3' and 5'-

502    GCATTGACCAGATCCTGTAGCATC-3'); *yap1* (5'-

503    TCCTTCGCAAGGCTTGGATAATTG-3' and 5'-

504    TTGTCTGGAGTGGGACTTTGGCTC-3'); *wwtr1* (5'-

505    GGACGAAAAACAGGAAAAGTTC-3' and 5'-ACTGCGGCATATCCTTGTTC-3').

506    These amplified PCR products were analyzed using MCE-202 MultiNA

507    microchip electrophoresis system (SHIMADZU, Kyoto, Japan) with the DNA-

508    500 reagent kit (SHIMADZU).

509

510    **Microinjection of oligonucleotide and mRNA**

511    We injected 200 pg *ytip-mCherry* mRNA (Fukui et al., 2014), 100 pg zebrafish-

512    *smad7* mRNA, 1.2 ng *lats1-atg* MO (5'-CCTCGGGTTTCTCGGCCCTCCTCAT-

513    3') (Chen et al., 2009a), 1.2 ng *lats2-atg* MO (5'-

514    CATGAGTGAACTTGGCCTGTTTTCT-3') (Chen et al., 2009a), 3 ng *pkd2-atg*

515    MO (5'-ACTGGAGTTCATCGTGTATTTCTAC-3') (Bisgrove et al., 2005), 8 ng

516    *ajuba-atg* MO (5'-TGAGTTTGATGCCAAGTCGATCCAT-3') (Witzel et al., 2012),

517    and 5 ng *control* MO (5'-CCTCTTACCTCAGTTACAATTTATA-3') as previously

eLIFE -Research article (Full Submission)-
Fukui et al.
30-05-2017-RA-eLife-29106

518    reported (Fukui et al., 2014). These morpholinos were purchased from Gene

519    Tools (Philomath, OR). Capped Messenger RNAs were synthesized using SP6

520    mMessage mMachine system (Thermo Fisher Scientific). Microinjection was

521    performed by using FemtoJet (Eppendorf, Hamburg, Germany). MOs, mRNA,

522    and Tol2 plasmids were injected into one-cell to two-cell stage blastomere.

523

524    **Heat shock treatment**

525    *TgBAC(hand2:GFP);Tg(myl7:Nls-mCherry)* embryos were injected with 25 pg

526    pTol2-*hsp70l*:GFP or 25 pg pTol2-*hsp70l*:bmp2b-2A-mCherry plasmids along

527    with 50 pg *tol2 transposase* mRNA and heat shocked at 2 ss for 1 hr at 39 °C.

528

529    **Mosaic assay**

530    Mosaic assay was performed as previously described (Fukui et al., 2014). For

531    injection of *smad7* mRNA into CPC-fated cells, *smad7* mRNA (4 pg) was co-

532    injected with *gata5* mRNA (1.5 pg) and *smarcd3b* mRNA (1.5 pg) together with

533    rhodamine dextran (70,000 MW, lysine fixable [Thermo Fisher Scientific]) as a

534    cell tracer into one blastomere at the 64 cell stage of *TgBAC(hand2:GFP)*

535    embryos. The *hand2* promoter-activated caudal region of the left ALPM of the

536    embryos was confocal imaged at 15 hpf (12 ss).

537

538    **EdU incorporation assay**

539    *TgBAC(isl1:GFP);Tg(myl7:Nls-mCherry)* embryos injected with *control* MO or

540    *lats1/2* MOs were incubated with 2 mM of 5-Ethynyl-2-deoxyuridine (EdU) from

541    14 to 26 hpf or 20 to 36 hpf, and subsequently fixed by 4% PFA at 96 hpf. EdU

eLIFE -Research article (Full Submission)-
Fukui et al.
30-05-2017-RA-eLife-29106

542 incorporated cells were labelled by Click-iT EdU Alexa Fluor 647 Imaging Kits

543 (Thermo Fisher Scientific) following manufacturer's instructions. Images were

544 taken by FV1200 confocal microscope system. The number of EdU-positive *isl1*

545 promoter-activated CMs were measured by the overlapping cell of Alexa Fluor

546 647-positive signal and *isl1* and *myl7* promoter-activated signals.

547

548 **Whole-mount in situ hybridization (WISH)**

549 The antisense *hand2, bmp2b, bmp4, gata4, nkx2.5, etv2, tal1, and hoxb5b* RNA

550 probes labeled with digoxigenin (DIG) were prepared by using an RNA labeling

551 kit (Roche, Basel, Switzerland). WISH was performed as previously described

552 (Fukui et al., 2014). Colorimetric reaction was carried out using BM purple

553 (Roche) as the substrate. To stop reaction, embryos were washed by PBS-T

554 and fixed by 4% PFA for 20 min at room temperature and subsequently

555 substituted by glycerol. Images were taken by SZX-16 Stereo Microscope

556 (Olympus).

557

558 **Immunohistochemistry**

559 Embryos at 26 hpf were fixed by MEMFA (3.7% formaldehyde, 0.1 M MOPS, 2

560 mM EGTA, 1 mM $MgSO_4$) for 2 hr at room temperature. After fixation, the

561 solution was changed to 50% Methanol / MEMFA for 10 min, changed to 100%

562 Methanol at room temperature, and stored in 100% Methanol at -30ºC

563 overnight. After rehydration, embryos were washed three-times for 10 min in

564 PBBT (PBS with 2 mg/mL BSA and 0.1% TritonX-100). Embryos were blocked

565 in PBBT with 10% goat serum for 60 min at room temperature, and

eLIFE -Research article (Full Submission)-
Fukui et al.
30-05-2017-RA-eLife-29106

566    subsequently incubated overnight at 4°C with primary antibodies, 1:300 diluted

567    chicken anti-GFP antibody (ab13970, Abcam, Cambridge, UK), 1:300 diluted

568    mouse anti-mCherry antibody (632543, Clontech, Mountain View, CA), and

569    1:100 diluted rabbit anti-Islet1 antibody (GTX128201, Genetex, Irvine, CA) or

570    1:100 diluted rabbit anti-pSmad1/5/9 antibody (13820S, Cell Signaling

571    TECHNOLOGY, Danvers, MA) in blocking solution. Embryos were washed with

572    PBBT for five-times over the course of 2 hours, with blocking solution for 60 min

573    at room temperature, and incubated overnight at 4°C with secondary antibodies,

574    anti-chicken Alexa Fluor 488 IgG (A-11039, Thermo Fisher Scientific), anti-

575    mouse Alexa Fluor 546 IgG (A-11030, Thermo Fisher Scientific), and anti-rabbit

576    Alexa Fluor 633 IgG (A-21070, Thermo Fisher Scientific) diluted 1:300 in

577    blocking solution. Embryos were washed with PBBT for five-times over the

578    course of 2 hours, and stored in PBS at 4°C prior to imaging.

579

580    **Quantitative real time PCR (q-PCR)**

581    Total RNAs were collected from whole-embryonic cells by using TRizol (Thermo

582    Fisher Scientific) following the manufacturer's instructions. For q-PCR, reverse

583    transcription and RT-PCR were performed with QuantiFast SYBR Green PCR

584    kit (Qiagen, Hilden, Germany) in Mastercycler Realplex (Eppendorf). The

585    following primer set were used for amplification: *nkx2.5*-S (5'-

586    GCTTTTACGCGAAGAACTTCC-3'), *nkx2.5*-AS (5'-

587    GATCTTCACCTGTGTGGAGG-3'); *gata4*-S (5'-AAGGTCATCCCGGTAAGCTC-

588    3'), *gata4*-AS (5'-TGTCACGTACACCGGAGAAG-3'); *hand2*-S (5'-

589    TACCATGGCACCTTCGTACA-3'), *hand2*-AS (5'-

eLIFE -Research article (Full Submission)-
Fukui et al.
30-05-2017-RA-eLife-29106

590    CCTTTCTTCTTTGGCGTCTG-3'); *eef1a1l1*-S (5'-

591    CTGGAGGCCAGCTCAAACAT-3'), *eef1a1l1*-AS (5'-

592    ATCAAGAAGAGTAGTACCGCTAGCATTAC-3') (Fukui et al., 2014).

593

594    **Plasmids**

595    cDNA fragments encoding zebrafish Hand2, Bmp2b, Bmp4, Gata4, Nkx2.5,

596    Etv2, Tal1, Hoxb5b and Smad7 were amplified by PCR using a cDNAs library

597    derived from zebrafish embryos and subcloned into pCR4 Blunt TOPO vector

598    (Thermo Fisher Scientific). The following primer set were used for amplification:

599    *hand2*-S (5'-CGGGATCCCGCCATGAGTTTAGTTGGAGGGTT-3' [containing

600    BamHI sequence]), *hand2*-AS (5'-GCTTTAGTCTCATTGCTTCAGTTCC-3');

601    *bmp2b*-S (5'-ATGTCGACACCATGGTCGCCGTGGTCCGCGCTCTC-3'

602    [containing SalI sequence]), *bmp2b*-AS (5'-

603    TCATCGGCACCCACAGCCCTCCACC-3'); *bmp4*-S (5'-

604    CGGGATCCCATGATTCCTGGTAATCGAATGC-3' [containing BamHI

605    sequence]), *bmp4*-AS (5'-CATTTGTACAACCTCCACAGCAAG-3'); *gata4*-S (5'-

606    GTGAATTCATGTATCAAGGTGTAACGATGGCC-3' [containing EcoRI

607    sequence]), *gata4*-AS (5'-GAGCTTCATGTAGAGTCCACATGC-3'); *nkx2.5*-S

608    (5'-GCTCTAGATTCCATGGCAATGTTCTCTAGCCAA-3' [containing XbaI

609    sequence]), *nkx2.5*-AS (5'-GATGAATGCTGTCGGTAAATGTAG-3'); *etv2*-S (5'-

610    GTGAATTCCTGGATTTTACACAGAAGACTTCAGA-3' [containing EcoRI

611    sequence]); *etv2*-AS (5'-CCACGACTGAGCTTCTCATAGTTC-3'); *tal1*-S (5'-

612    GTGAATTCGAAATCCGAGCAATTTCCGCTGAG-3' [containing EcoRI

613    sequence]), *tal1*-AS (5'-CTTAGCATCTCCTGAAGGAGGTCGT-3'); *hoxb5b*-S

27

eLIFE -Research article (Full Submission)-
Fukui et al.
30-05-2017-RA-eLife-29106

614    (5'-GTGAATTCCCAAATGAGCTCTTATTTTCTAAACTCG-3' [containing EcoRI

615    sequence]), *hoxb5b*-AS (5'-GATGTGATTTGATCAATTTTGAAACGCGC-3');

616    *smad7*-S (5'-AGGGATCCTCCCGCATGTTCAGGACCAAACGAT-3' [containing

617    BamHI sequence]), *smad7*-AS (5'-

618    GAAGGCCTTTATCGGTTATTAAATATGACCTCTAACC-3' [containing StuI

619    sequence]). The cDNAs of zYtip, Gata5, and Smarcd3b were previously

620    amplified and cloned into the pCS2 vector (Clontech) (Fukui et al., 2014). The

621    DNA encoding Smad7 was subcloned into the pCS2 vector to construct the

622    pCS2-smad7. pTol2-*hsp70l* was previously reported (Kashiwada et al., 2015).

623    The cDNAs encoding GFP and Bmp2b-2A-mCherry were subcloned into the

624    pTol2-*hsp70l* vector to construct the pTol2-*hsp70l*:GFP and pTol2-

625    *hsp70l*:bmp2b-2A-mCherry. All the cDNAs amplified by PCR using cDNA

626    libraries were sequenced. Mutations were also confirmed by sequencing.

627

628    **Generation of Transgenic Lines**

629    To monitor the atrial CM development, we established a transgenic (Tg)

630    zebrafish lines expressing nuclear localization signal (Nls)-tagged tandem Eos

631    fluorescent protein under the control of *myosin heavy chain 6* (*myh6*) promoter;

632    *Tg*(*myh6:Nls-tdEosFP*). pTol2-*myh6* vector was constructed by modifying pTol2

633    vector and inserting the *myh6* promoter as a driver of expression of the target

634    molecule. The primers to amplify the *myh6* promoter were 5'-

635    AGAGCTAAAGTGGCAGTGTGCCGAT-3' and 5'-

636    TCCCGAACTCTGCCATTAAAGCATCAC-3'. An oligonucleotide encoding Nls

637    derived from SV40 (PKKKRKV) was inserted into pcDNA-tdEosFP (MoBiTec,

28

eLIFE -Research article (Full Submission)-
Fukui et al.
30-05-2017-RA-eLife-29106

638    Göttingen, Germany) to generate the plasmids expressing Nls-tagged tandem

639    Eos fluorescent protein (Nls-tdEosFP). The Nls-tdEosFP cDNA was subcloned

640    into the pTol2-*myh6* vector to construct the pTol2-*myh6*:Nls-tdEosFP plasmids.

641        To monitor the CM-specific Yap1/Wwtr1-dependent transcriptional

642    activation, we developed a Tg line which expresses human (h) TEAD2 lacking

643    amino-terminus (1-113 aa) fused with Gal4 DNA binding domain followed by 2A

644    mCherry under the control of *myosin light polypeptide 7* (*myl7*) promoter;

645    *Tg(myl7:galdb-hTEAD2ΔN-2A-mCherry).* This Tg fish was crossed with

646    *Tg(uas:GFP)* reporter fish to obtain *Tg(myl7:galdb-hTEAD2ΔN-2A-*

647    *mCherry);Tg(uas:GFP).* The pTol2-*myl7* vector and the pcDNA3.1 vector

648    containing human *TEAD2ΔN* cDNA fused to the DNA binding domain of Gal4

649    (pcDNA3.1-galdb-hTEAD2ΔN) were constructed as previously described (Fukui

650    et al., 2014). The Gal4db-hTEAD2ΔN cDNA was subcloned into the pTol2-*myl7*

651    vector to construct the pTol2-*myl7*:galdb-hTEAD2ΔN plasmids. All the cDNAs

652    amplified by PCR using cDNA libraries were confirmed by sequence.

653        To monitor the SHF development, we established a Tg line which expresses

654    GFP under the control of *isl1* BAC promoter/enhancer; *TgBAC(isl1:GFP).*

655    pRedET plasmid (Gene Bridges, Heidelberg, Germany) was introduced into E.

656    coli containing CH211-219F7 BAC clone encoding *isl1* gene (BacPAC

657    resources) by electroporation (1800V, 25 mF, 200 Ω) to increase the efficiency

658    of homologous recombination, as previously described (Ando et al., 2016). Tol2

659    long terminal repeats in opposite directions flanking ampicillin resistance

660    cassette were amplified by PCR using Tol2_amp as a template and were

661    inserted into the BAC vector backbone. The cDNA encoding GFP together with

29

eLIFE -Research article (Full Submission)-
Fukui et al.
30-05-2017-RA-eLife-29106

662 a kanamycin resistance cassette (GFP_KanR) was amplified by PCR using

663 pCS2-GFP_KanR plasmid as a template and inserted into the start ATG of the

664 *isl1* gene. Primers to amplify the GFP_KanR for *isl1* gene were 5'-

665 gggccttctgtccggttttaaaagtggacctaacaccgccttactttcttACCATGGTGAGCAAGGGC

666 GAGGAG-3' and 5'-

667 aaataaacaataaagcttaacttacttttcggtggatcccccatgtctccTCAGAAGAACTCGTCAAG

668 AAGGCG-3' (small letters; homology arm to BAC vector, and capital letters;

669 primer binding site to the template plasmid).

670 Tol2-mediated zebrafish transgenesis was performed by injecting 30 pg

671 transgene plasmid together with 50 pg *Tol2* mRNA, followed by subsequent

672 screening of F1 founders and establishment of single-insertion transgenic

673 strains through selection in F3 generations.

674

675 **Data analysis and statistics**

676 Data were analyzed using GraphPad Prism 7 (GraphPad Software, La Jolla,

677 CA). All columns were indicated as mean ± SEM. Statistical significance of

678 multiple groups was determined by one-way ANOVA with Bonferroni's post hoc

679 test. The number of atrial and ventricular CMs at 74 hpf were analyzed by

680 Student's t-test. Statistical significance of two groups was determined by

681 Student's t-test.

682

683 **Acknowledgements**

eLIFE -Research article (Full Submission)-
Fukui et al.
30-05-2017-RA-eLife-29106

## References

Abu-Issa R, Kirby ML. 2008. Patterning of the heart field in the chick. *Developmental Biology* **319**: 223-233. doi: 10.1016/j.ydbio.2008.04.014, PMID: 18513714

Ando K, Fukuhara S, Izumi N, Nakajima H, Fukui H, Kelsh RN, Mochizuki N. 2016. Clarification of mural cell coverage of vascular endothelial cells by live imaging of zebrafish. *Development* **143**: 1328-1339. doi: 10.1242/dev.132654, PMID: 26952986

Asakawa K, Suster ML, Mizusawa K, Nagayoshi S, Kotani T, Urasaki A, Kishimoto Y, Hibi M, Kawakami K. 2008. Genetic dissection of neural circuits by Tol2 transposon-mediated Gal4 gene and enhancer trapping in zebrafish. *Proceedings of the National Academy of Sciences of the United States of America* **105**: 1255-1260. doi: 10.1073/pnas.0704963105, PMID: 18202183

Bisgrove BW, Snarr BS, Emrazian A, Yost HJ. 2005. Polaris and Polycystin-2 in dorsal forerunner cells and Kupffer's vesicle are required for specification of the zebrafish left-right axis. *Developmental Biology* **287**: 274-288. doi: 10.1016/j.ydbio.2005.08.047, PMID: 16216239

Cai CL, Liang X, Shi Y, Chu PH, Pfaff SL, Chen J, Evans S. 2003. Isl1 identifies a cardiac progenitor population that proliferates prior to differentiation and contributes a majority of cells to the heart. *Developmental Cell* **5**: 877-889. PMID: 14667410

Caputo L, Witzel HR, Kolovos P, Cheedipudi S, Looso M, Mylona A, van IJcken WF, Laugwitz KL, Evans SM, Braun T, Soler E, Grosveld F, Dobreva G. 2015. The Isl1/Ldb1 Complex Orchestrates Genome-wide Chromatin Organization to Instruct Differentiation of Multipotent Cardiac Progenitors. *Cell Stem Cell* **17**: 287-299. doi: 10.1016/j.stem.2015.08.007, PMID: 26321200

Chen CH, Sun YH, Pei DS, Zhu ZY. 2009. Comparative expression of zebrafish lats1 and lats2 and their implication in gastrulation movements. *Developmental Dynamics* **238**: 2850-2859. doi: 10.1002/dvdy.22105, PMID: 19842174

Chen L, Fulcoli FG, Tang S, Baldini A. 2009. Tbx1 regulates proliferation and

eLIFE -Research article (Full Submission)-
Fukui et al.
30-05-2017-RA-eLife-29106

717   differentiation of multipotent heart progenitors. *Circulation Research* **105**: 842-
718   851. doi: 10.1161/CIRCRESAHA.109.200295, PMID: 19745164

719   Chung WS, Shin CH, Stainier DY. 2008. Bmp2 signaling regulates the hepatic
720   versus pancreatic fate decision. *Developmental Cell* **15**: 738-748. doi:
721   10.1016/j.devcel.2008.08.019, PMID: 19000838

722   Collery RF, Link BA.2011. Dynamic smad-mediated BMP signaling revealed
723   through transgenic zebrafish. *Developmental Dynamics* **240**: 712-722. doi:
724   10.1002/dvdy.22567, PMID: 21337469

725   de Pater E, Ciampricotti M, Priller F, Veerkamp J, Strate I, Smith K, Lagendijk
726   AK, Schilling TF, Herzog W, Abdelilah-Seyfried S, Hammerschmidt M, Bakkers
727   J. 2012. Bmp signaling exerts opposite effects on cardiac differentiation.
728   *Circulation Research* **110**: 578-587. doi: 10.1161/CIRCRESAHA.111.261172,
729   PMID: 22247485

730   de Pater E, Clijsters L, Marques SR, Lin YF, Garavito-Aguilar ZV, Yelon D,
731   Bakkers J. 2009. Distinct phases of cardiomyocyte differentiation regulate
732   growth of the zebrafish heart. *Development* **136**: 1633-1641. doi:
733   10.1242/dev.030924, PMID: 19395641

734   Fishman MC, Chien KR. 1997. Fashioning the vertebrate heart: earliest
735   embryonic decisions. *Development* **124**: 2099-2117, PMID: 9187138

736   Fukui H, Terai K, Nakajima H, Chiba A, Fukuhara S, Mochizuki N. 2014. S1P-
737   Yap1 signaling regulates endoderm formation required for cardiac precursor cell
738   migration in zebrafish. *Developmental Cell* **31**: 128-136. doi:
739   10.1016/j.devcel.2014.08.014, PMID: 25313964

740   Galli D, Dominguez JN, Zaffran S, Munk A, Brown NA, Buckingham ME. 2008.
741   Atrial myocardium derives from the posterior region of the second heart field,
742   which acquires left-right identity as Pitx2c is expressed. *Development* **135**:
743   1157-1167. doi: 10.1242/dev.014563, PMID: 18272591

744   Guner-Ataman B, Paffett-Lugassy N, Adams MS, Nevis KR, Jahangiri L,
745   Obregon P, Kikuchi K, Poss KD, Burns CE, Burns CG. 2013. Zebrafish second
746   heart field development relies on progenitor specification in anterior lateral plate
747   mesoderm and nkx2.5 function. *Development* **140**: 1353-1363. doi:

eLIFE -Research article (Full Submission)-
Fukui et al.
30-05-2017-RA-eLife-29106

748    10.1242/dev.088351, PMID: 23444361

749    Gupta S, Zhu H, Zon LI, Evans T. 2006. BMP signaling restricts hemato-
750    vascular development from lateral mesoderm during somitogenesis.
751    *Development* **133**: 2177-2187. doi: 10.1242/dev.02386, PMID: 16672337

752    Hami D, Grimes AC, Tsai HJ, Kirby ML. 2011. Zebrafish cardiac development
753    requires a conserved secondary heart field. *Development* **138**: 2389-2398. doi:
754    10.1242/dev.061473, PMID: 21558385

755    Heldin CH, Miyazono K, ten DP. 1997. TGF-beta signalling from cell membrane
756    to nucleus through SMAD proteins. *Nature* **390**: 465-471. doi: 10.1038/37284,
757    PMID: 9393997

758    Hinits Y, Pan L, Walker C, Dowd J, Moens CB, Hughes SM. 2012. Zebrafish
759    Mef2ca and Mef2cb are essential for both first and second heart field
760    cardiomyocyte differentiation. *Developmental Biology* **369**: 199-210. doi:
761    10.1016/j.ydbio.2012.06.019, PMID: 22750409

762    Huang Z, Hu J, Pan J, Wang Y, Hu G, Zhou J, Mei L, Xiong WC. 2016. YAP
763    stabilizes SMAD1 and promotes BMP2-induced neocortical astrocytic
764    differentiation. *Development* **143**: 2398-2409. doi: 10.1242/dev.130658, PMID:
765    27381227

766    Kashiwada T, Fukuhara S, Terai K, Tanaka T, Wakayama Y, Ando K, Nakajima
767    H, Fukui H, Yuge S, Saito Y, Gemma A, Mochizuki N. 2015. β-catenin-
768    dependent transcription is central to Bmp-mediated formation of venous
769    vessels. *Development* **142**: 497-509. doi: 10.1242/dev.115576. PMID: 25564648

770    Kelly RG, Buckingham ME, Moorman AF. 2014. Heart fields and cardiac
771    morphogenesis. *Cold Spring Harbor Perspectives in Medicine* **4**. a015750. doi:
772    10.1101/cshperspect.a015750, PMID: 25274757

773    Kimmel CB, Warga RM, Schilling TF. 1990. Origin and organization of the
774    zebrafish fate map. *Development* **108**: 581-594. PMID: 2387237

775    Kishimoto Y, Lee KH, Zon L, Hammerschmidt M, Schulte-Merker S. 1997. The
776    molecular nature of zebrafish swirl: BMP2 function is essential during early
777    dorsoventral patterning. *Development* **124**: 4457-4466. PMID: 9409664

eLIFE -Research article (Full Submission)-
Fukui et al.
30-05-2017-RA-eLife-29106

778  Lazic S, Scott IC. 2011. Mef2cb regulates late myocardial cell addition from a
779  second heart field-like population of progenitors in zebrafish. *Developmental*
780  *Biology* **354**: 123-133. doi: 10.1016/j.ydbio.2011.03.028, PMID: 21466801

781  Lin Z, von GA, Zhou P, Gu F, Ma Q, Jiang J, Yau AL, Buck JN, Gouin KA, van
782  Gorp PR, Zhou B, Chen J, Seidman JG, Wang DZ, Pu WT. 2014. Cardiac-
783  specific YAP activation improves cardiac function and survival in an
784  experimental murine MI model. *Circulation Research* **115**: 354-363. doi:
785  10.1161/CIRCRESAHA.115.303632, PMID: 24833660

786  Lou X, Deshwar AR, Crump JG, Scott IC. 2011. Smarcd3b and Gata5 promote
787  a cardiac progenitor fate in the zebrafish embryo. *Development* **138**: 3113-3123.
788  doi: 10.1242/dev.064279, PMID: 21715426

789  Mudumana SP, Hentschel D, Liu Y, Vasilyev A, Drummond IA. 2008. odd
790  skipped related1 reveals a novel role for endoderm in regulating kidney versus
791  vascular cell fate. *Development* **135**: 3355-3367. doi: 10.1242/dev.022830,
792  PMID: 18787069

793  Nakajima H, Yamamoto K, Agarwala S, Terai K, Fukui H, Fukuhara S, Ando K,
794  Miyazaki T, Yokota Y, Schmelzer E, Belting HG, Affolter M, Lecaudey V,
795  Mochizuki N. 2017. Flow-Dependent Endothelial YAP Regulation Contributes to
796  Vessel Maintenance. *Developmental Cell* **40**: 523-536. doi:
797  10.1016/j.devcel.2017.02.019, PMID: 28350986

798  Nishioka N, Inoue K, Adachi K, Kiyonari H, Ota M, Ralston A, Yabuta N,
799  Hirahara S, Stephenson RO, Ogonuki N, Makita R, Kurihara H, Morin-Kensicki
800  EM, Nojima H, Rossant J, Nakao K, Niwa H, Sasaki H. 2009. The Hippo
801  signaling pathway components Lats and Yap pattern Tead4 activity to
802  distinguish mouse trophectoderm from inner cell mass. *Developmental Cell* **16**:
803  398-410. doi: 10.1016/j.devcel.2009.02.003, PMID: 19289085

804  Prall OW, Menon MK, Solloway MJ, Watanabe Y, Zaffran S, Bajolle F, Biben C,
805  McBride JJ, Robertson BR, Chaulet H, Stennard FA, Wise N, Schaft D,
806  Wolstein O, Furtado MB, Shiratori H, Chien KR, Hamada H, Black BL, Saga Y,
807  Robertson EJ, Buckingham ME, Harvey RP. 2007. An Nkx2-5/Bmp2/Smad1
808  negative feedback loop controls heart progenitor specification and proliferation.
809  *Cell* **128**: 947-959. doi: 10.1016/j.cell.2007.01.042, PMID: 17350578

eLIFE -Research article (Full Submission)-
Fukui et al.
30-05-2017-RA-eLife-29106

810  Schindler YL, Garske KM, Wang J, Firulli BA, Firulli AB, Poss KD, Yelon D.
811  2014. Hand2 elevates cardiomyocyte production during zebrafish heart
812  development and regeneration. *Development* **141**: 3112-3122. doi:
813  10.1242/dev.106336, PMID: 25038045

814  Schlueter J, Manner J, Brand T. 2006. BMP is an important regulator of
815  proepicardial identity in the chick embryo. *Developmental Biology* **295**: 546-558.
816  doi: 10.1016/j.ydbio.2006.03.036, PMID: 16677627

817  Schoenebeck JJ, Keegan BR, Yelon D. 2007. Vessel and blood specification
818  override cardiac potential in anterior mesoderm. *Developmental Cell* **13**: 254-
819  267. doi: 10.1016/j.devcel.2007.05.012, PMID: 17681136

820  Souchelnytskyi S, Nakayama T, Nakao A, Moren A, Heldin CH, Christian JL, ten
821  DP. 1998. Physical and functional interaction of murine and Xenopus Smad7
822  with bone morphogenetic protein receptors and transforming growth factor-beta
823  receptors. *Journal of Biological Chemistry* **273**: 25364-25370. PMID: 9738003

824  Staudt D, Stainier D. 2012. Uncovering the molecular and cellular mechanisms
825  of heart development using the zebrafish. *Annual Reviews of Genetics* **46**: 397-
826  418. doi: 10.1146/annurev-genet-110711-155646, PMID: 22974299

827  Tirosh-Finkel L, Zeisel A, Brodt-Ivenshitz M, Shamai A, Yao Z, Seger R,
828  Domany E, Tzahor E. 2010. BMP-mediated inhibition of FGF signaling
829  promotes cardiomyocyte differentiation of anterior heart field progenitors.
830  *Development* **137**: 2989-3000. doi: 10.1242/dev.051649, PMID: 20702560

831  Verzi MP, McCulley DJ, De VS, Dodou E, Black BL. 2005. The right ventricle,
832  outflow tract, and ventricular septum comprise a restricted expression domain
833  within the secondary/anterior heart field. *Developmental Biology* **287**: 134-145.
834  doi: 10.1016/j.ydbio.2005.08.041, PMID: 16188249

835  von Gise A, Lin Z, Schlegelmilch K, Honor LB, Pan GM, Buck JN, Ma Q,
836  Ishiwata T, Zhou B, Camargo FD, Pu WT. 2012. YAP1, the nuclear target of
837  Hippo signaling, stimulates heart growth through cardiomyocyte proliferation but
838  not hypertrophy. *Proceedings of the National Academy of Sciences of the*
839  *United States of America* **109**: 2394-2399. doi: 10.1073/pnas.1116136109,
840  PMID: 22308401

eLIFE -Research article (Full Submission)-
Fukui et al.
30-05-2017-RA-eLife-29106

841 Waxman JS, Keegan BR, Roberts RW, Poss KD, Yelon D. 2008. Hoxb5b acts
842 downstream of retinoic acid signaling in the forelimb field to restrict heart field
843 potential in zebrafish. *Developmental Cell* **15**: 923-934. doi:
844 10.1016/j.devcel.2008.09.009, PMID: 19081079

845 Witzel HR, Cheedipudi S, Gao R, Stainier DY, Dobreva GD. 2017. Isl2b
846 regulates anterior second heart field development in zebrafish. *Scientific*
847 *Reports* **7**: 41043. doi: 10.1038/srep41043, PMID: 28106108

848 Witzel HR, Jungblut B, Choe CP, Crump JG, Braun T, Dobreva G. 2012. The
849 LIM protein Ajuba restricts the second heart field progenitor pool by regulating
850 Isl1 activity. *Developmental Cell* **23**: 58-70. doi: 10.1016/j.devcel.2012.06.005,
851 PMID: 22771034

852 Xin M, Kim Y, Sutherland LB, Murakami M, Qi X, McAnally J, Porrello ER,
853 Mahmoud AI, Tan W, Shelton JM, Richardson JA, Sadek HA, Bassel-Duby R,
854 Olson EN. 2013. Hippo pathway effector Yap promotes cardiac regeneration.
855 *Proceedings of the National Academy of Sciences of the United States of*
856 *America* **110**: 13839-13844. doi: 10.1073/pnas.1313192110, PMID: 23918388

857 Yang L, Cai CL, Lin L, Qyang Y, Chung C, Monteiro RM, Mummery CL,
858 Fishman GI, Cogen A, Evans S. 2006. Isl1Cre reveals a common Bmp pathway
859 in heart and limb development. *Development* **133**: 1575-1585. doi:
860 10.1242/dev.02322, PMID: 16556916

861 Yin C, Kikuchi K, Hochgreb T, Poss KD, Stainier DY. 2010. Hand2 regulates
862 extracellular matrix remodeling essential for gut-looping morphogenesis in
863 zebrafish. *Developmental Cell* **18**: 973-984. doi: 10.1016/j.devcel.2010.05.009,
864 PMID: 20627079

865 Zhao B, Ye X, Yu J, Li L, Li W, Li S, Yu J, Lin JD, Wang CY, Chinnaiyan AM, Lai
866 ZC, Guan KL. 2008. TEAD mediates YAP-dependent gene induction and growth
867 control. *Genes and Development* **22**: 1962-1971. doi: 10.1101/gad.1664408,
868 PMID: 18579750

869 Zhou Q, Li L, Zhao B, Guan KL. 2015. The hippo pathway in heart
870 development, regeneration, and diseases. *Circulation Research* **116**: 1431-
871 1447. doi: 10.1161/CIRCRESAHA.116.303311, PMID: 25858067

eLIFE -Research article (Full Submission)-
Fukui et al.
30-05-2017-RA-eLife-29106

872   Zhou Y, Cashman TJ, Nevis KR, Obregon P, Carney SA, Liu Y, Gu A, Mosimann

873   C, Sondalle S, Peterson RE, Heideman W, Burns CE, Burns CG. 2011. Latent

874   TGF-beta binding protein 3 identifies a second heart field in zebrafish. *Nature*

875   **474**: 645-648. doi: 10.1038/nature10094, PMID: 21623370

876

877

878

eLIFE -Research article (Full Submission)-
Fukui et al.
30-05-2017-RA-eLife-29106

879
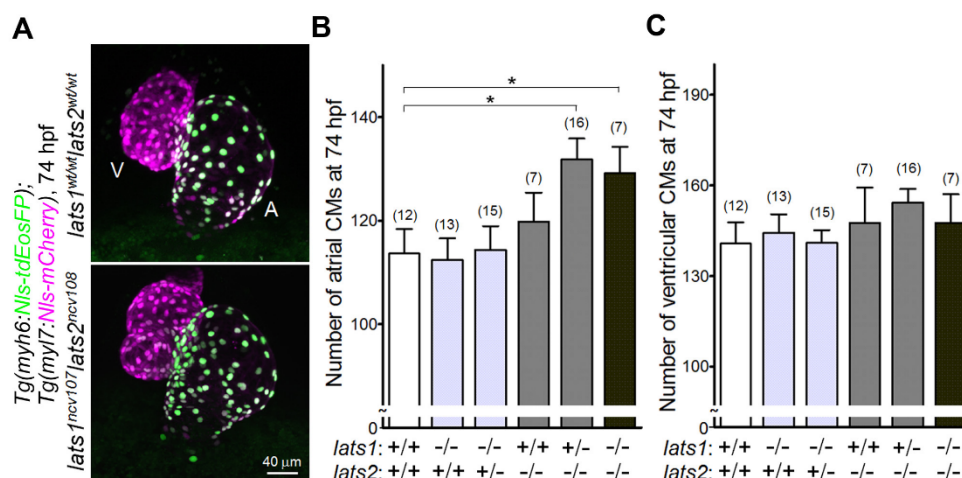
880 **Figure 1.** Knockout of *lats1/2* genes leads to an increase of the number of atrial, but not

881 ventricular CMs during early development. **(A)** 3D confocal stack images of *Tg(myh6:Nls-*

882 *tdEosFP);Tg(myl7:Nls-mCherry)* embryos at 74 hpf of the *lats1$^{wt/wt}$lats2$^{wt/wt}$* (top) and *the*

883 *lats1$^{ncv107}$lats2$^{ncv108}$* (bottom). Atrial (A) and ventricular (V) cardiomyocytes (CMs) are EosFP-

884 positive cells and EosFP-negative mCherry-positive cells, respectively. Ventral view, anterior to

885 the top. The confocal 3D-stack images are a set of representative images of eight independent

886 experiments. **(B, C)** Quantitative analyses of the number of atrial **(B)** and ventricular **(C)** CMs of

887 the embryos at 74 hpf with alleles indicated at the bottom. Plus (+) and minus (-) indicate the *wt*

888 allele and the allele of *ncv107* or *ncv108* in *lats1* or *lats2* genes, respectively. In the following

889 graphs, total number of larvae examined in the experiment is indicated on the top of column

890 unless otherwise described. $^{*}p < 0.05$.

891

892 The following figure supplements are available for figure 1:

893 **Figure supplement 1.** Knockout of *lats1/2* genes leads to an activation of the Tead reporter.

894 **Figure supplement 2.** Tead reporter activation is found in the venous pole CMs of atrium.

895

896 **Figure 1—source data 1. Quantification of atrial (Figure 1B) and ventricular (Figure 1C)**

897 **cardiomyocyte numbers in the embryos with *lats1* and *lats2* mutant.**

898

899

eLIFE -Research article (Full Submission)-
Fukui et al.
30-05-2017-RA-eLife-29106
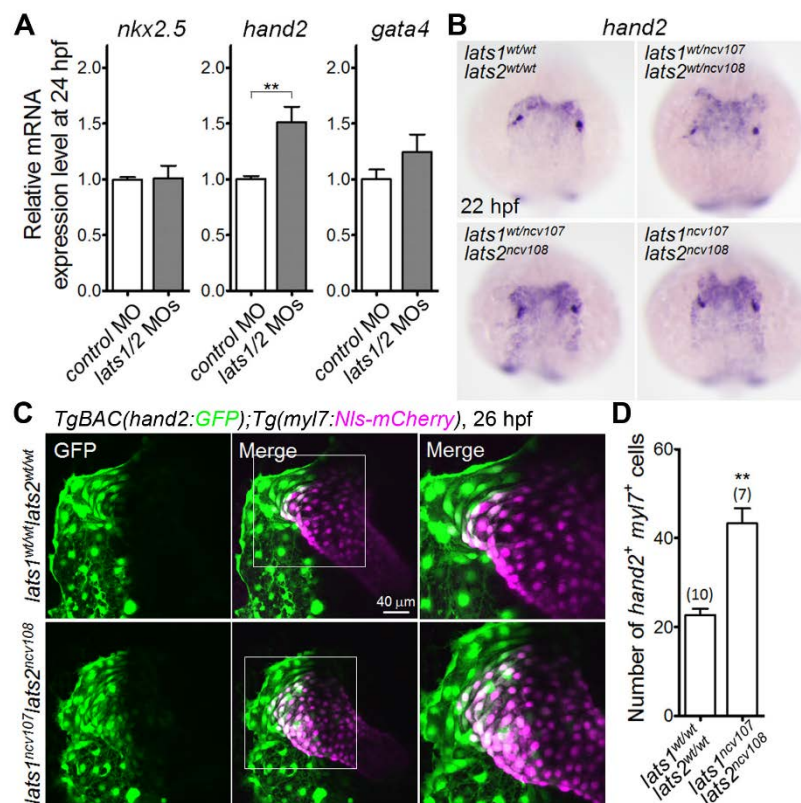


**Figure 2.** Knockout of *lats1/2* results in an increase in the both *myl7* and *hand2* promoter-activated cells in the venous pole. **(A)** Quantitative-PCR analyses of expression of *nkx2.5*, *hand2*, and *gata4* mRNAs in the whole embryos at 24 hpf injected with the morpholino (MO) indicated at the bottom (n=4). Relative expression of mRNA in the morphants to that of the control is calculated. **(B)** Whole mount in situ hybridization (WISH) analyses of the embryos at 22 hpf of the *lats1^{wt/wt}lats2^{wt/wt}*, *lats1^{wt/ncv107}lats2^{wt/ncv108}*, *lats1^{wt/ncv107}lats2^{ncv108}* and the *lats1^{ncv107}lats2^{ncv108}* indicated at the top using antisense probe for *hand2*. **(C)** 3D confocal stack images of the *TgBAC(hand2:GFP);Tg(myl7:Nls-mCherry)* embryos of the *lats1^{wt/wt}lats2^{wt/wt}* (upper panels) and *the lats1^{ncv107}lats2^{ncv108}* (bottom panels) at 26 hpf. GFP images (left), merged images of GFP image and mCherry image (center), and enlarged images of boxed regions in the center panels (right). **(D)** Quantitative analysis of the number of both *hand2* and *myl7* promoter-activated cells at 26 hpf. All images in Figure 2 are dorsal view, anterior to the top. The confocal 3D-stack images and ISH images are a set of representative images of at least four independent experiments. $^{**}p < 0.01$.

The following figure supplements are available for figure 2:

**Figure supplement 1.** Depletion of Lats1/2 results in an increase in the *hand2* promoter-activated cells in the venous pole.

39

eLIFE -Research article (Full Submission)-
Fukui et al.
30-05-2017-RA-eLife-29106

919    **Figure supplement 2.** *hand2* promoter-activated cells were significantly reduced in the

920    *yap1/wwtr1* double-knockout embryos.

921

922    **Figure 2—source data 1. Quantification of the relative mRNAs expression levels (Figure**

923    **2A) and the number of both *hand2* and *myl7* promoter-activated cells (Figure 2D).**

924

eLIFE -Research article (Full Submission)-
Fukui et al.
30-05-2017-RA-eLife-29106
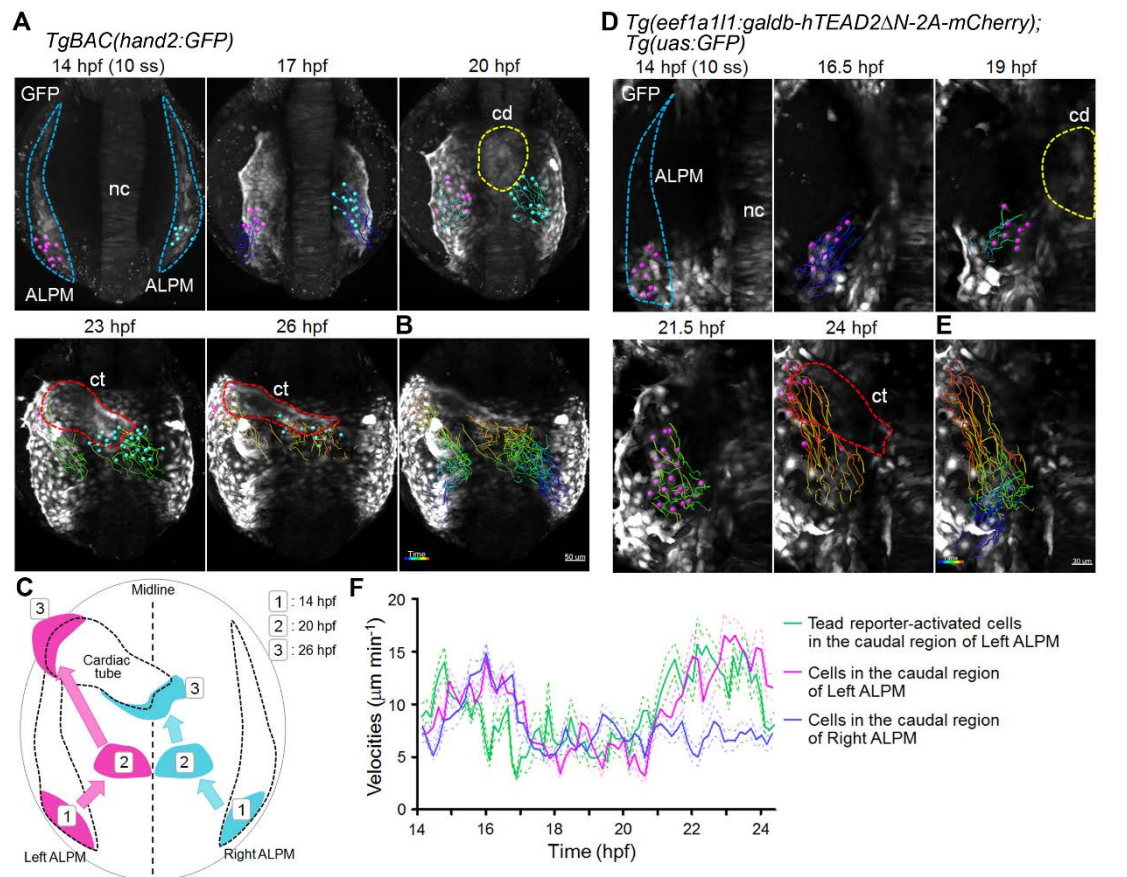
**Figure 3.** Tead transcription-activated cells in the caudal region of the left ALPM move to venous pole **(A, B)** Time-sequential 3D-rendered confocal images of a *TgBAC*(*hand2:GFP*) embryo from 14 hpf (10 ss) to 26 hpf as indicate at the top. Spots of magenta and cyan denote the cells in the caudal part of left and right ALPM, respectively. **(B)** Tracking of caudal end *hand2* promoter-activated ALPM cells from 14 hpf to 26 hpf. The color of the tracks changes from blue to red according to the time after imaging (0 h to 12 h). Notochord, nc; cardiac disc, cd; cardiac tube, ct. ALPM, cd, and ct are marked by the blue, yellow, and red broken lines, respectively. **(C)** Schematic illustration of trajectory patterns of the caudal end ALPM cells from 14 hpf to 26 hpf. Magenta and cyan denote the region of caudal region of left and right ALPM, respectively. The cells in the caudal region of left (magenta) and right (cyan) ALPM moved from the region 1 (14 hpf) to the region 3 (26 hpf) through the region 2 (20 hpf). **(D, E)** Time-sequential 3D-rendered confocal images of a *Tg(eef1a1l1:galdb-hTEAD2ΔN-2A-mCherry);Tg(uas:GFP)* embryo from 14 hpf (10 ss) to 24 hpf. Spots of magenta denote the Tead reporter-activated cells in the caudal region of the left ALPM. **(E)** Tracking of Tead reporter-activated cells from 14 hpf to 24 hpf. The color of the tracks changes from blue to red according to the time after imaging (0 h to 10 h). **(F)** Mean velocities of movement of *hand2* promoter-activated cells in the caudal region of left (magenta) and right (blue) ALPM and that of Tead
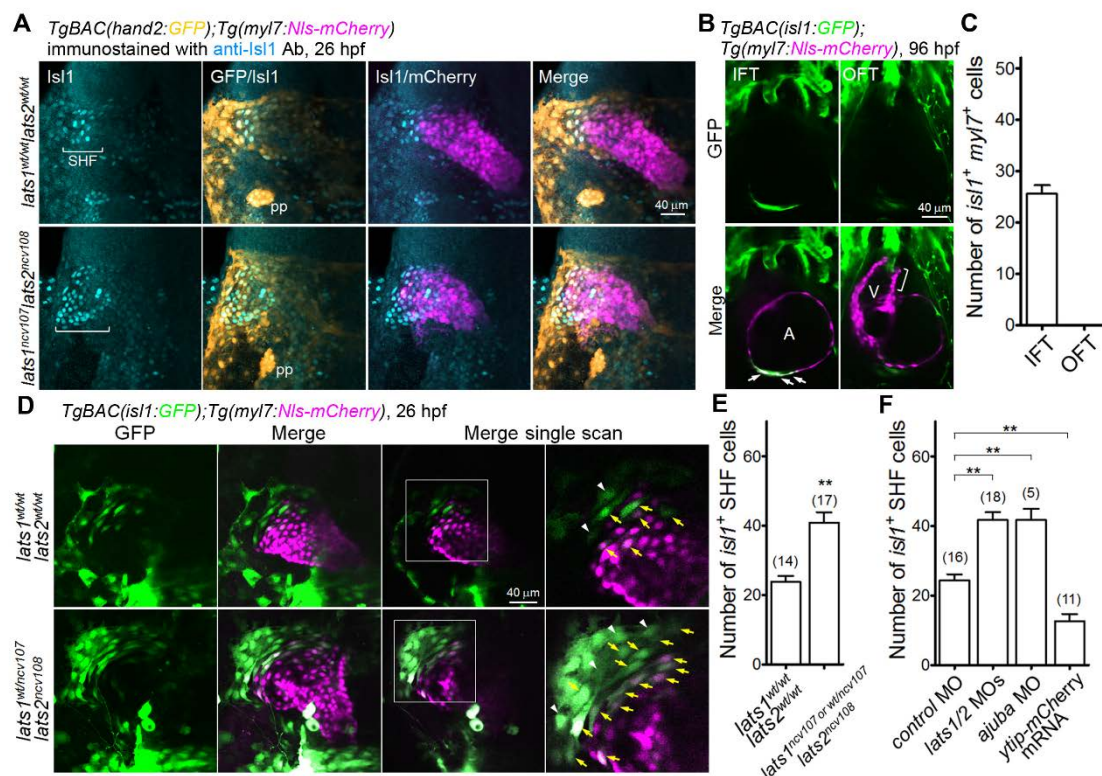
eLIFE -Research article (Full Submission)-
Fukui et al.
30-05-2017-RA-eLife-29106

943 reporter-activated cells in the caudal region of the left ALPM (green) from 14 hpf to 24 hpf.

944 Broken lines indicate the SEM of the mean line. All images in Figure 3 are dorsal view, anterior

945 to the top. The confocal 3D-stack images are a set of representative images of six independent

946 experiments.

947

948 The following figure supplement is available for figure 3:

949 **Figure supplement 1.** Cells in the caudal region of right ALPM of the *pkd2* morphants with situs

950 inversus migrate toward the right-sided venous pole.

951

952 **Figure 3—source data 1. Quantification of mean velocities of *hand2* promoter-activated**

953 **cells and Tead reporter-activated cells in the caudal region of left and right ALPM.**

954

eLIFE -Research article (Full Submission)-
Fukui et al.
30-05-2017-RA-eLife-29106

955

**Figure 4.** Hippo signaling is involved in the formation of the Isl1-positive SHF cells in the venous pole. **(A)** 3D confocal stack images of the *TgBAC(hand2:GFP);Tg(myl7:Nls-mCherry)* embryos with *lats1^{wt/wt}lats2^{wt/wt}* allele (upper panels) and *lats1^{ncv107}lats2^{ncv108}* allele (bottom panels) immunostained with anti-Isl1 antibody (anti-Isl1 Ab) at 26 hpf. Brackets denote the SHF cells that are Isl1-positive and both *hand2* and *myl7* promoter-activated cells and that are Isl1-positive and *hand2* promoter-activated cells in contact with *myl7* promoter-activated cells. pp indicates the pharyngeal pouch that expresses *hand2* promoter-activated GFP signal. Dorsal view, anterior to the top. The first, second, third and fourth images are Isl-1 immunostaining, the merged image of GFP image and Isl1 immunostaining, the merged image of Isl1 immunostaining and mCherry image, and the merged of all the three (GFP, mCherry, and Isl1 immunostaining), respectively. **(B)** Single-scan confocal images of the *TgBAC(isl1:GFP);Tg(myl7:Nls-mCherry)* embryos at 96 hpf. Both *isl1* and *myl7* promoter-activated cells are in the inflow tract (IFT) cells (arrows) but not in the outflow tract (OFT) cells (bracket). A, atrium; V, ventricle. Ventral view, anterior to the top. The confocal images are a set of representative images of four independent experiments. **(C)** Quantitative analyses of the number of both *isl1* and *myl7* promoter-activated cells in the IFT and OFT at 96 hpf (n=10). **(D)** Confocal images of the *TgBAC(isl1:GFP);Tg(myl7:Nls-mCherry)* embryos of the *lats1^{wt/wt}lats2^{wt/wt}* and the *lats1^{wt/ncv107}lats2^{ncv108}* at 26 hpf. The boxed regions are enlarged in the most right panels. Yellow arrows indicate both *isl1* and *myl7* promoter-activated cells in the
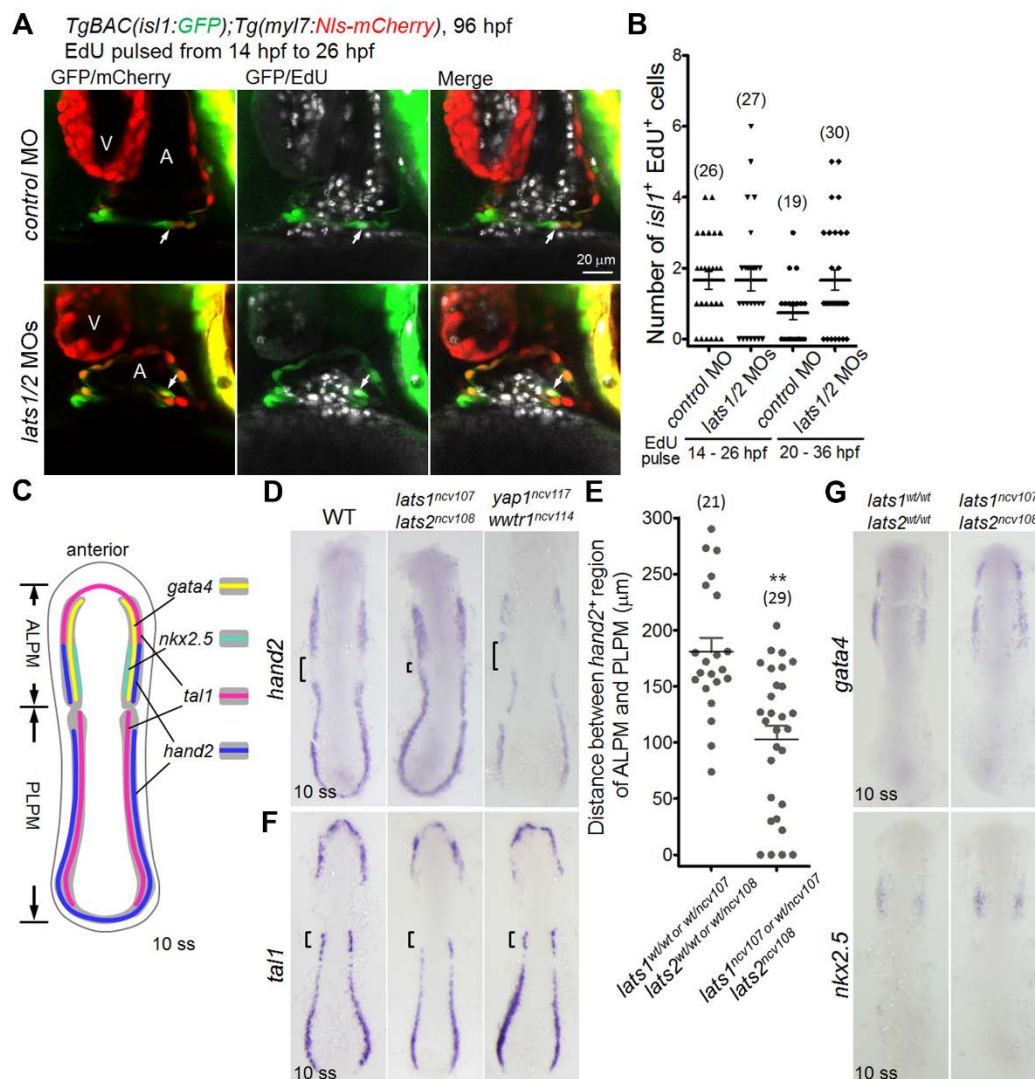
43

eLIFE -Research article (Full Submission)-
Fukui et al.
30-05-2017-RA-eLife-29106

975    venous pole. White arrowheads indicate the *isl1* promoter-activated cells in contact with *myl7*

976    promoter-activated cells. 3D confocal stack images (left two panels) and single-scan images

977    (right two panels). Dorsal view, anterior to the top. **(E, F)** Quantitative analyses of the number of

978    the *isl1* promoter-activated SHF cells in the venous pole of *lats1^{wt/wt}lats2^{wt/wt}* embryos and either

979    *lats1^{wt/ncv107}lats2^{ncv108}* embryos or *lats1/2* DKO embryos **(E)**, and embryos shown in Figure 4—

980    Figure supplement 1E **(F)**. Both *isl1* and *myl7* promoter-activated cells and *isl1* promoter-

981    activated cells in contact with *myl7* promoter-activated cell were counted as SHF cells. The

982    confocal 3D-stack images and single-scan (2 $\mu$m) images are a set of representative images of

983    at least four independent experiments. [**]$p < 0.01$.

984

985    The following figure supplement is available for figure 4:

986    **Figure supplement 1.** Depletion of Lats1/2 leads to an increase of the number of Isl1-positive

987    SHF cells in the venous pole.

988

989    **Figure 4—source data 1. The number of *isl1* and *myl7* promoter-activated IFT and OFT**

990    **cells at 96 hpf (Figure 4C) and *isl1* promoter-activated SHF cells of *lat1/2* mutants (Figure**

991    **4E) and *lat1/2* morphants (Figure 4F) at 26 hpf.**

992

993

eLIFE -Research article (Full Submission)-
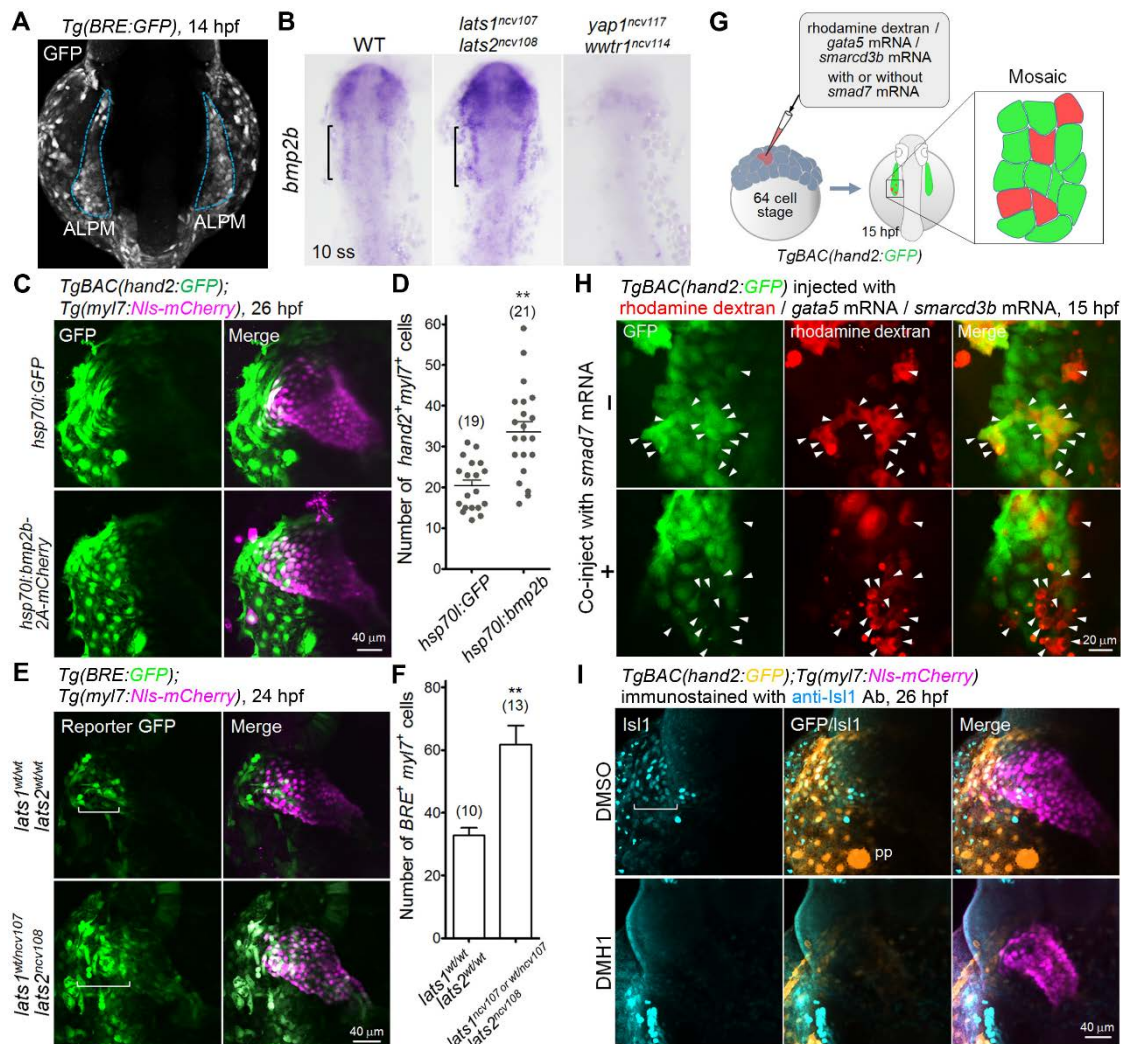Fukui et al.
30-05-2017-RA-eLife-29106



**Figure 5.** Knockout of *lats1/2* leads to an increase in the expression of *hand2* in the boundary between ALPM and PLPM. **(A)** Single-scan confocal images of the *TgBAC(isl1:GFP);Tg(myl7:Nls-mCherry)* embryos injected with the MO indicated at the left and pulsed with EdU from 14 hpf to 26 hpf at 96 hpf. Arrows indicate the EdU-incorporated both *isl1* and *myl7* promoter-activated cells in the IFT of atrium. A, atrium; V, ventricle. Ventral view, anterior to the top. **(B)** The number of EdU-positive *isl1* promoter-activated CMs among EdU-positive cells of the embryos treated with the MO as indicated at the bottom. Embryos pulsed with EdU from 14 hpf to 26 hpf (left two columns) and from 20 hpf to 36 hpf (right two columns). **(C)** Schematic illustration of gene expression patterns in the LPM of the wild type (WT) embryos at 10 somite stage (ss). Expression domain of *tal1, gata4, nkx2.5, and hand2* are depicted as magenta, yellow, green, and blue, respectively. Dorsal view, anterior to the top. **(D, F, G)** WISH analyses of the embryos at 10 ss using antisense probe indicated at the left of the panels. **(D, F)** Genotypes are indicated at the top as WT (left panels), *lats1/2* DKO (center panels), and

eLIFE -Research article (Full Submission)-
Fukui et al.
30-05-2017-RA-eLife-29106

1008    *yap1/wwtr1* DKO (right panels). **(D)** Brackets indicate the gap between *hand2*-positive regions

1009    of ALPM and PLPM. **(E)** Quantitative measurement of the distance indicated by the brackets of

1010    **(D)** in the either *lats1$^{wt/wt}$ lats2$^{wt/wt}$* or *lats1 $^{wt/ncv107}$ lats2 $^{wt/ncv108}$* embryos and either

1011    *lats1$^{wt/ncv107}$lats2$^{ncv108}$* embryos or *lats1/2* DKO embryos. **(F)** Brackets indicate the *tal1*-positive

1012    rostral end of PLPM in the WT. **(G)** Genotypes are indicated at the top as WT (left panels), and

1013    *lats1/2* DKO (right panels). Dorsal view, anterior to the top. The single-scan (2 $\mu$m) confocal

1014    images and ISH images are a set of representative images of at least four independent

1015    experiments. $^{**}$p < 0.01.

1016

1017    The following figure supplement is available for figure 5:

1018    **Figure supplement 1.** Depletion of Lats1/2 leads to an increase in the expression of *hand2*.

1019

1020    **Figure 5—source data 1.   Distance between *hand2*-positive regions of ALPM and PLPM**

1021    **of the control and the *lat1/2* mutants at 10 ss.**

1022

46

eLIFE -Research article (Full Submission)-
Fukui et al.
30-05-2017-RA-eLife-29106

**Figure 6.** Hippo signaling functions upstream of Bmp-Smad signal that is necessary for Isl1-positive SHF formation. **(A)** 3D confocal stack images of the *Tg(BRE:GFP)* embryos at 14 hpf. Blue broken lines indicate the GFP-positive ALPM. **(B)** WISH analyses of the embryos at 10 ss of the WT, *lats1/2* DKO, and *yap1/wwtr1* DKO indicated at the top using antisense probe for *bmp2b*. Brackets indicate the *bmp2b*-positive ALPM. **(C)** 3D confocal stack images of the *TgBAC(hand2:GFP);Tg(myl7:Nls-mCherry)* embryos injected with pTol2-*hsp70l*:GFP and pTol2-*hsp70l*:bmp2b-2A-mCherry and treated by heat shock at 2 ss for 1 h at 26 hpf. **(D)** Quantitative analyses of the number of both *hand2* and *myl7* promoter-activated cells in the venous pole. Note that overexpression of bmp2b leads to an increase in the number of the *hand2* promoter-activated cardiomyocytes in the venous pole. **(E)** 3D confocal stack images of the *Tg(BRE:GFP);Tg(myl7:Nls-mCherry)* embryos with *lats1^{wt/wt}lats2^{wt/wt}* allele and *lats1^{wt/ncv107}lats2^{ncv108}* allele at 24 hpf. Brackets indicate the GFP-positive *myl7* promoter-activated cells in the venous pole. Note that GFP-positive *myl7* promoter-activated cells are increased in the venous pole. **(F)** Quantitative analyses of the number of the both *BRE-*

47

eLIFE -Research article (Full Submission)-
Fukui et al.
30-05-2017-RA-eLife-29106

1038    activated GFP-positive and *myl7* promoter-activated mCherry-positive cells in the

1039    *lats1^{wt/wt}lats2^{wt/wt}* embryos and either *lats1^{wt/ncv107}lats2^{ncv108}* embryos or *lats1/2* DKO embryos.

1040    **(G)** Schematic illustration of mosaic analysis. CPC-fated cells by the injection of *gata5* and

1041    *smarcd3b* mRNAs were simultaneously injected with *smad7* mRNA and rhodamine dextran into

1042    one blastomere at 64 cell stage of *TgBAC(hand2:GFP)* embryos. At 15 hpf, the caudal region of

1043    the left ALPM was imaged by confocal microscopy. **(H)** 3D confocal stack images of the

1044    *TgBAC(hand2:GFP)* embryos injected with rhodamine dextran, *gata5* mRNA, *smarcd3b* mRNA

1045    without *smad7* mRNA (upper panels) and with *smad7* mRNA (bottom panels) at 15 hpf.

1046    Arrowheads indicate the rhodamine dextran-labelled cells in the caudal region of the left ALPM.

1047    Note that *hand2* promoter-activated GFP signal was suppressed in the cells that express *smad7*

1048    mRNA. **(I)** 3D confocal stack images of the *TgBAC(hand2:GFP);Tg(myl7:Nls-mCherry)* embryos

1049    treated with DMSO (upper panels) or DMH1 (10 μM, bottom panels) from 14 hpf to 26 hpf and

1050    immunostained with anti-Isl1 Ab at 26 hpf. Bracket indicates Isl1-positive cells in the venous

1051    pole. All images in Figure 6 are dorsal view, anterior to the top. Note that both *hand2* and *myl7*

1052    promoter-activated and Isl1-positive cells in the venous pole are absent in the embryos treated

1053    with DMH1. The confocal 3D-stack images and ISH images are a set of representative images

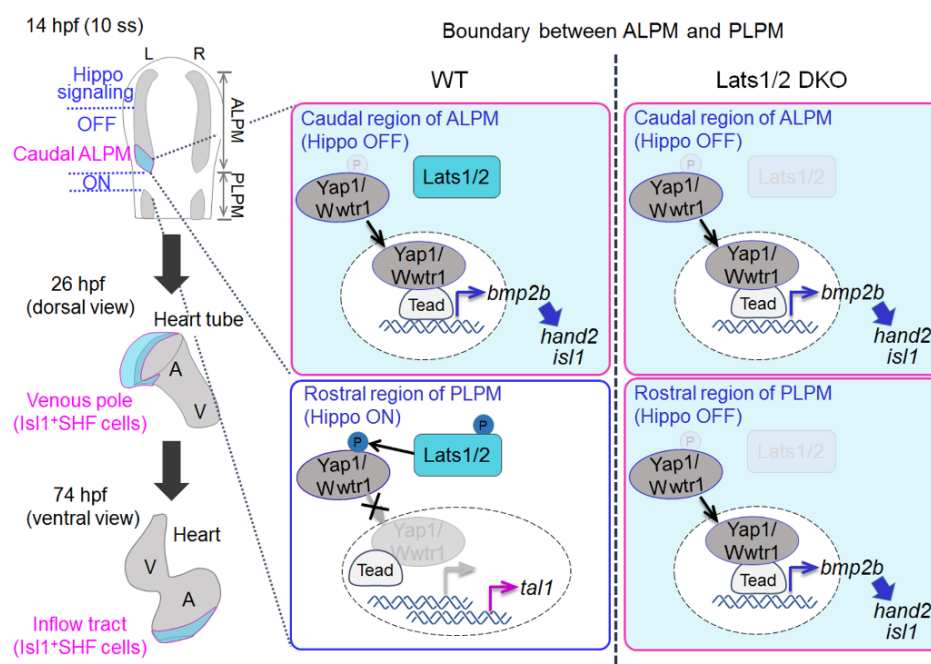1054    of at least four independent experiments. $^{**}p < 0.01$.

1055

1056    The following figure supplements are available for figure 6:

1057    **Figure supplement 1.** Depletion of Lats1/2 leads to an increase in the *bmps* expression.
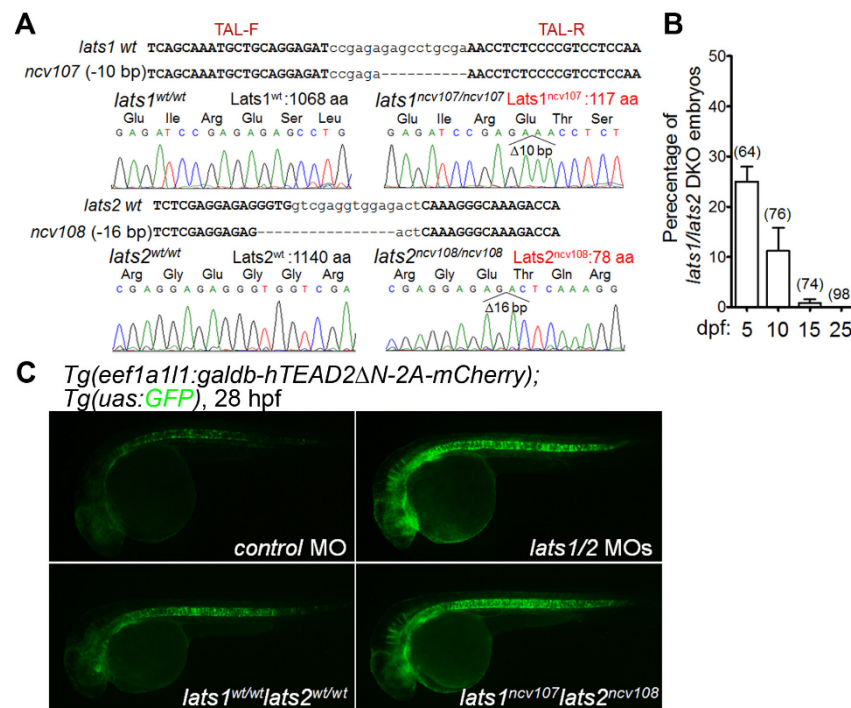
1058    **Figure supplement 2.** Depletion of Lats1/2 leads to an activation of Bmp-Smad signaling that is

1059    necessary for Isl1-positive SHF formation.

1060

1061    **Figure 6—source data 1. The number of both *hand2* and *myl7* promoter-activated cells at**

1062    **26 hpf (Figure 6D) and BRE-positive cardiomyocytes of the lat1/2 mutants at 24 hpf**

1063    **(Figure 6F).**

1064

1065

eLIFE -Research article (Full Submission)-
Fukui et al.
30-05-2017-RA-eLife-29106



**Figure 7.** A schematic representation of inflow tract atrial CMs development from the caudal region of the left ALPM. Our study suggest that Lats1/2-Yap1/Wwtr1 signaling controls *bmp2b* expression in the ALPM. Secreted Bmp2b activates Smad signaling that cell autonomously induces the expression of *hand2* to differentiate Isl1 positive SHF cells in the caudal region of the left ALPM. In the *lats1/2* DKO embryos, Yap1/Wwtr1 facilitate Tead-dependent *bmp2b* expression, and thereby expands the expression of *hand2* caudally at the expense of *tal1* expression in the rostral region of PLPM. Consequently, hippo signaling restricts the number of the venous pole cells and lately inflow tract atrial CMs by regulating Bmp-Smad signaling in the boundary between ALPM and PLPM.

eLIFE -Research article (Full Submission)-
Fukui et al.
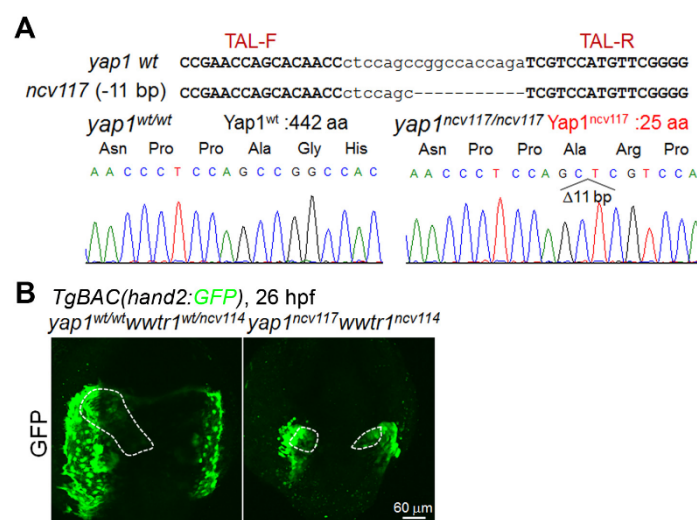30-05-2017-RA-eLife-29106

**Figure 1—Figure supplement 1.** Knockout of *lats1/2* genes leads to an activation of the Tead reporter. **(A)** *lats1* and *lats2* gene mutation by TALEN at the targeted loci. A deletion of ten base pairs in the *ncv107* allele and sixteen base pairs in the *ncv108* allele results in a premature stop codon in exon 3 of *lats1* (resulting mutant Lats1 consists of 117 aa) and exon 3 of *lats2* (resulting mutant Lats2 consists of 78 aa), respectively. Upper and lower case letters denote target and spacer region for the TALEN, respectively. **(B)** The number of double knockout (DKO) embryos by incrossing of *lats1wt/ncv107lats2ncv108* fishes at the days post-fertilization (dpf) indicated at the bottom. Total number of larvae examined in the experiment is indicated on the top of column. **(C)** Fluorescent images of *Tg(eef1a1l1:galdb-hTEAD2ΔN-2A-mCherry);Tg(uas:GFP)* embryos injected with *control* MO and *lats1/2* MOs (upper panels), and with *lats1wt/wtlats2wt/wt* allele and *lats1ncv107lats2ncv108* allele (bottom panels) at 28 hpf. Lateral view, anterior to the left. The fluorescent images **(C)** are a set of representative images of four independent experiments.
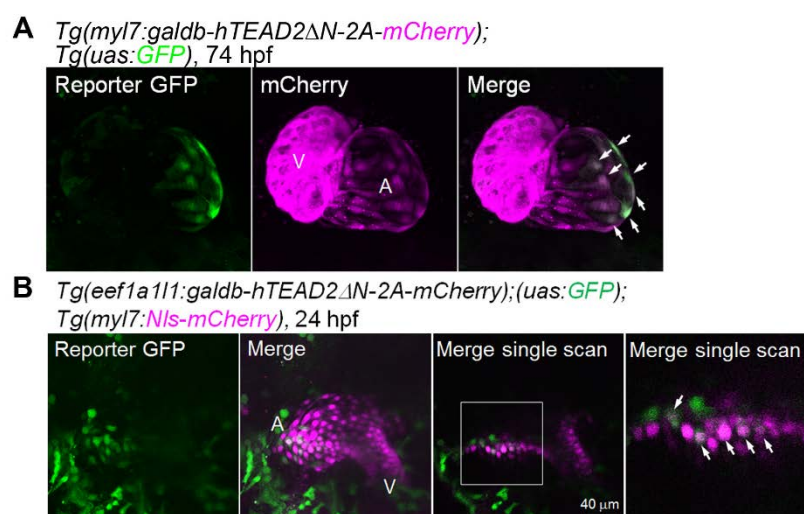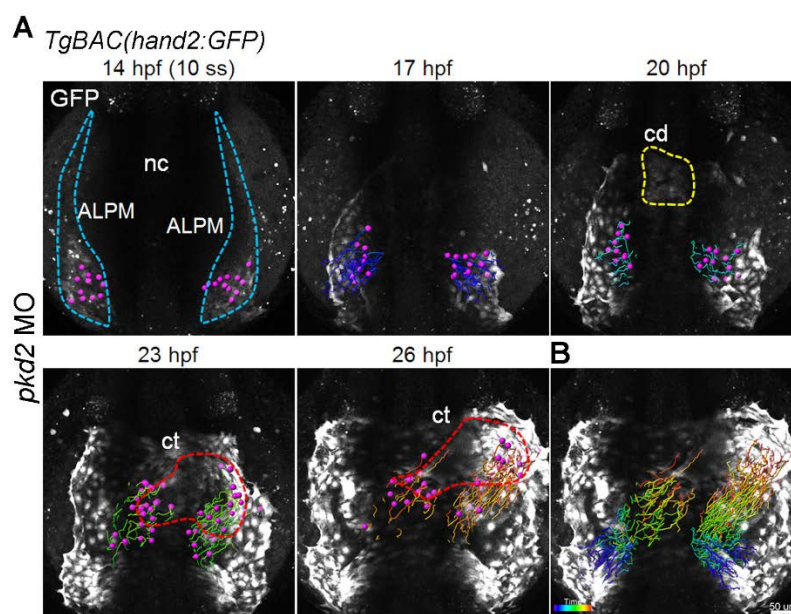
eLIFE -Research article (Full Submission)-
Fukui et al.
30-05-2017-RA-eLife-29106



1093

**Figure 1—Figure supplement 2.** Tead reporter activation is found in the venous pole CMs of
atrium. **(A)** 3D confocal stack images of *Tg*(*myl7:galdb-hTEAD2ΔN-2A-mCherry);Tg(uas:GFP*)
embryos at 74 hpf. Arrows indicate the TEAD reporter GFP-positive atrial CMs. Reporter GFP
image (left), mCherry image (center), and merged image of GFP and mCherry (right). A, atrium;
V, ventricle. Ventral view, anterior to the top. **(B)** Confocal images of *Tg(eef1a1l1:galdb-*
*hTEAD2ΔN-2A-mCherry);Tg(uas:GFP*);*Tg(myl7:Nls-mCherry)* embryos at 24 hpf. The boxed
region is enlarged and shown in the most right panel. Arrows indicate the Tead reporter-positive
cells that might differentiate into atrial CMs. Regions in the heart tube that would give rise to
atrium (A) and ventricle (V) are marked. 3D-stack images (left two panels) and single scan
images (right two panels). Dorsal view, anterior to the top. The confocal 3D-stack images are a
set of representative images of at least four independent experiments.

1105

eLIFE -Research article (Full Submission)-
Fukui et al.
30-05-2017-RA-eLife-29106



1106
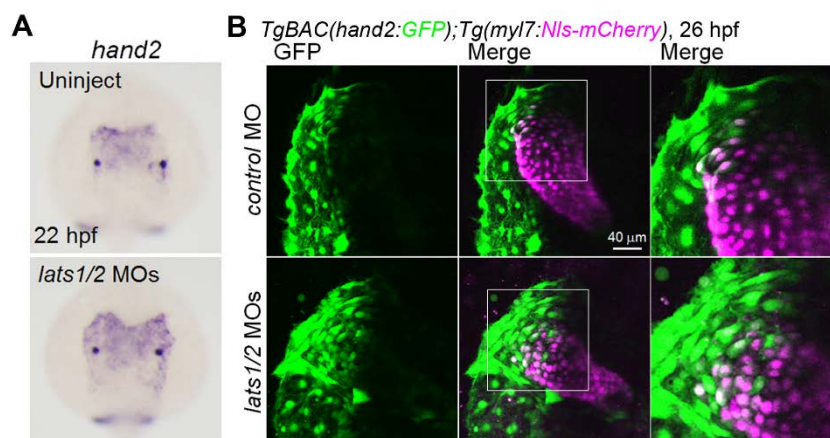
1107 **Figure 2—Figure supplement 1.** Depletion of Lats1/2 results in an increase in the *hand2*

1108 promoter-activated cells in the venous pole. **(A)** Whole mount in situ hybridization (WISH)

1109 analyses of the embryos at 22 hpf of the control (uninject) and injected with the *lats1/2* MOs

1110 indicated at the top using antisense probe for *hand2*. **(B)** 3D confocal stack images of

1111 *TgBAC(hand2:GFP);Tg(myl7:Nls-mCherry)* embryos injected with *control* MO and *lats1/2* MOs

1112 at 26 hpf. GFP images (left), merged images of GFP image and mCherry image (center), and

1113 enlarged images of boxed regions in the center panels (right). Dorsal view, anterior to the top.

1114 Images are a set of representative images of eight independent experiments.

1115

1116

eLIFE -Research article (Full Submission)-
Fukui et al.
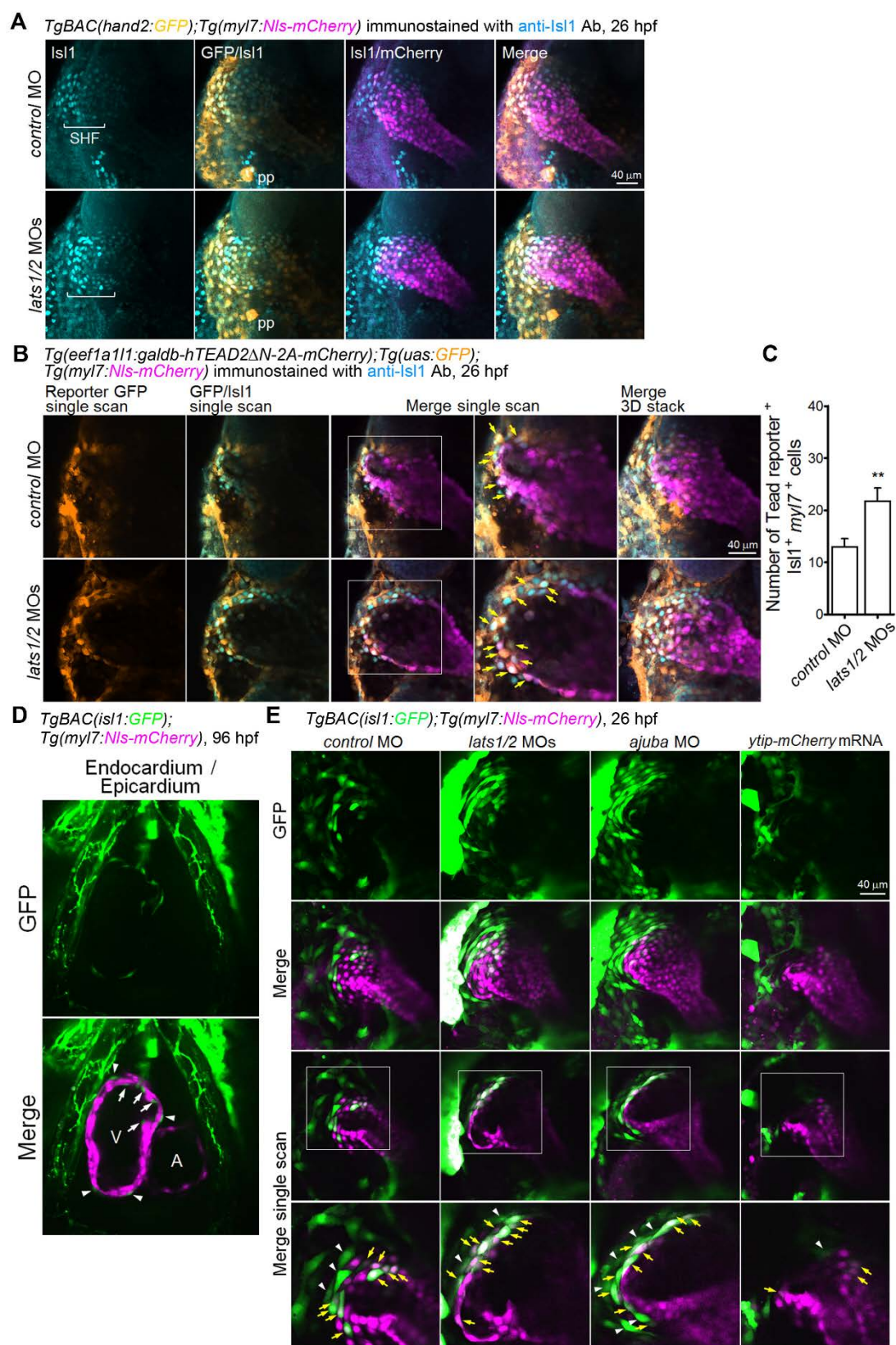30-05-2017-RA-eLife-29106



1117

1118 **Figure 2—Figure supplement 2.** *hand2* promoter-activated cells were significantly reduced in

1119 the *yap1/wwtr1* double-knockout embryos. **(A)** *yap1* gene mutation by TALEN at the targeted

1120 loci. A deletion of eleven base pairs in the *ncv117* allele results in a premature stop codon in

1121 exon 1 of *yap1* (resulting mutant Yap1 consists of 25 aa). Upper and lower case letters denote

1122 target and spacer regions for the TALEN, respectively.

1123 **(B)** 3D confocal stack images of *TgBAC(hand2:GFP)* embryos of the *yap1^{wt/wt}wwtr1^{wt/ncv114}* (left)

1124 and the *yap1^{ncv117}wwtr1^{ncv114}* (right) at 26 hpf. Dotted lines indicate the heart region. Note the

1125 CPCs located bilaterally in the *yap1^{ncv117}wwtr1^{ncv114}* embryos. The confocal 3D-stack images are

1126 a set of representative images of three independent experiments.

1127

1128

53

eLIFE -Research article (Full Submission)-
Fukui et al.
30-05-2017-RA-eLife-29106

1129

**Figure 3—Figure supplement 1.** Caudal region of right ALPM migrate toward the venous pole of reversed-heart tube in the *pkd2* morphant. **(A)** Time-sequential 3D-rendered confocal images of a *TgBAC*(*hand2:GFP*) embryo injected with *pkd2* MO from 14 hpf (10 ss) to 26 hpf as indicate at the top. Spots of magenta denote the cells in the caudal part of left and right ALPM. **(B)** Tracking of caudal end *hand2* promoter-activated ALPM cells from 14 hpf to 26 hpf. The color of the tracks changes from blue to red according to the time after imaging (0 h to 12 h). Notochord, nc; cardiac disc, cd; cardiac tube, ct. ALPM, cd, and ct are marked by the blue, yellow, and red broken lines, respectively. The confocal 3D-stack images are a set of representative images of four independent experiments.
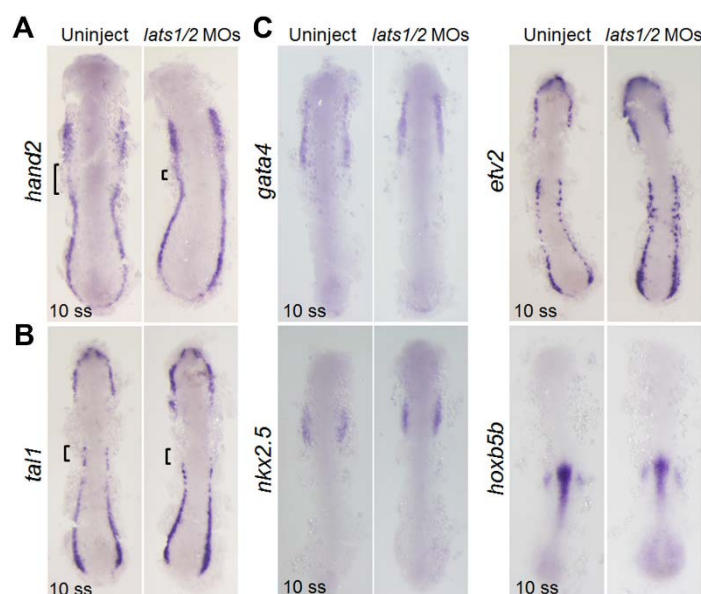
eLIFE -Research article (Full Submission)-
Fukui et al.
30-05-2017-RA-eLife-29106

**A** *TgBAC(hand2:GFP);Tg(myl7:Nls-mCherry)* immunostained with anti-Isl1 Ab, 26 hpf

**B** *Tg(eef1a1l1:galdb-hTEAD2ΔN-2A-mCherry);Tg(uas:GFP); Tg(myl7:Nls-mCherry)* immunostained with anti-Isl1 Ab, 26 hpf

**C**

**D** *TgBAC(isl1:GFP); Tg(myl7:Nls-mCherry)*, 96 hpf

**E** *TgBAC(isl1:GFP);Tg(myl7:Nls-mCherry)*, 26 hpf

1139     **Figure 4—Figure supplement 1.** Depletion of Lats1/2 leads to an increase of the number of

eLIFE -Research article (Full Submission)-
Fukui et al.
30-05-2017-RA-eLife-29106

1140   Isl1-positive SHF cells in the venous pole. **(A)** 3D confocal stack images of

1141   *TgBAC*(*hand2:GFP*)*;Tg(myl7:Nls-mCherry*) embryos injected with MO indicated at the left and

1142   immunostained with anti-Isl1 antibody (Ab) at 26 hpf. Brackets denote the SHF cells that are

1143   Isl1-positive and both *hand2* and *myl7* promoter-activated cells and those in contact with *myl7*

1144   promoter-activated cell. The first, second, third and fourth images are Isl-1 immunostaining, the

1145   merged image of GFP image and Isl1 immunostaining, the merged image of Isl1

1146   immunostaining and mCherry image, and the merged of all the three (GFP, mCherry, and Isl1

1147   immunostaining), respectively. pp indicates the pharyngeal pouch that expresses *hand2*

1148   promoter-activated GFP signals. Dorsal view, anterior to the top. **(B)** Confocal images of

1149   *Tg(eef1a1l1:galdb-hTEAD2ΔN-2A-mCherry);Tg(uas:GFP);Tg(myl7:Nls-mCherry)* embryos

1150   injected with the MO indicated at the left and immunostained with anti-Isl1 Ab at 26 hpf. The

1151   boxed regions in the center panels are enlarged in the next right panels. Tead reporter-

1152   dependent GFP-positive cells in the Isl1-positive *myl7* promoter-activated cells (yellow arrows)

1153   are observed in the venous pole. 3D confocal stack images (the most right panels) and single

1154   scan images (left four panels). Dorsal view, anterior to the top. **(C)** Quantitative analyses of the

1155   number of Isl1-positive *myl7* promoter-activated cells that are positive for Tead reporter-

1156   dependent GFP in the venous pole of **(B)** (n=5). **p < 0.01. **(D)** Single-scan confocal images of

1157   the *TgBAC(isl1:GFP);Tg(myl7:Nls-mCherry)* embryos at 96 hpf. GFP-positive mCherry-negative

1158   cells in the inside (arrows) and outside (arrowheads) of *myl7* promoter-positive ventricular CMs

1159   are endocardial cells and epicardial cells, respectively. A, atrium; V, ventricle. Ventral view,

1160   anterior to the top. **(E)** Confocal images of the *TgBAC(isl1:GFP);Tg(myl7:Nls-mCherry)* embryos

1161   injected with the MO and mRNA at 26 hpf. The boxed regions are enlarged in the bottom

1162   panels. Yellow arrows indicate both *isl1* and *myl7* promoter-activated cells in the venous pole.

1163   White arrowheads indicate the *isl1* promoter-activated cells in contact with *myl7* promoter-

1164   activated cells. 3D confocal stack images (upper two panels) and single-scan images (bottom

1165   two panels). Dorsal view, anterior to the top. The confocal 3D-stack images and single-scan

1166   images are a set of representative images of at least three independent experiments.

1167

1168

eLIFE -Research article (Full Submission)-
Fukui et al.
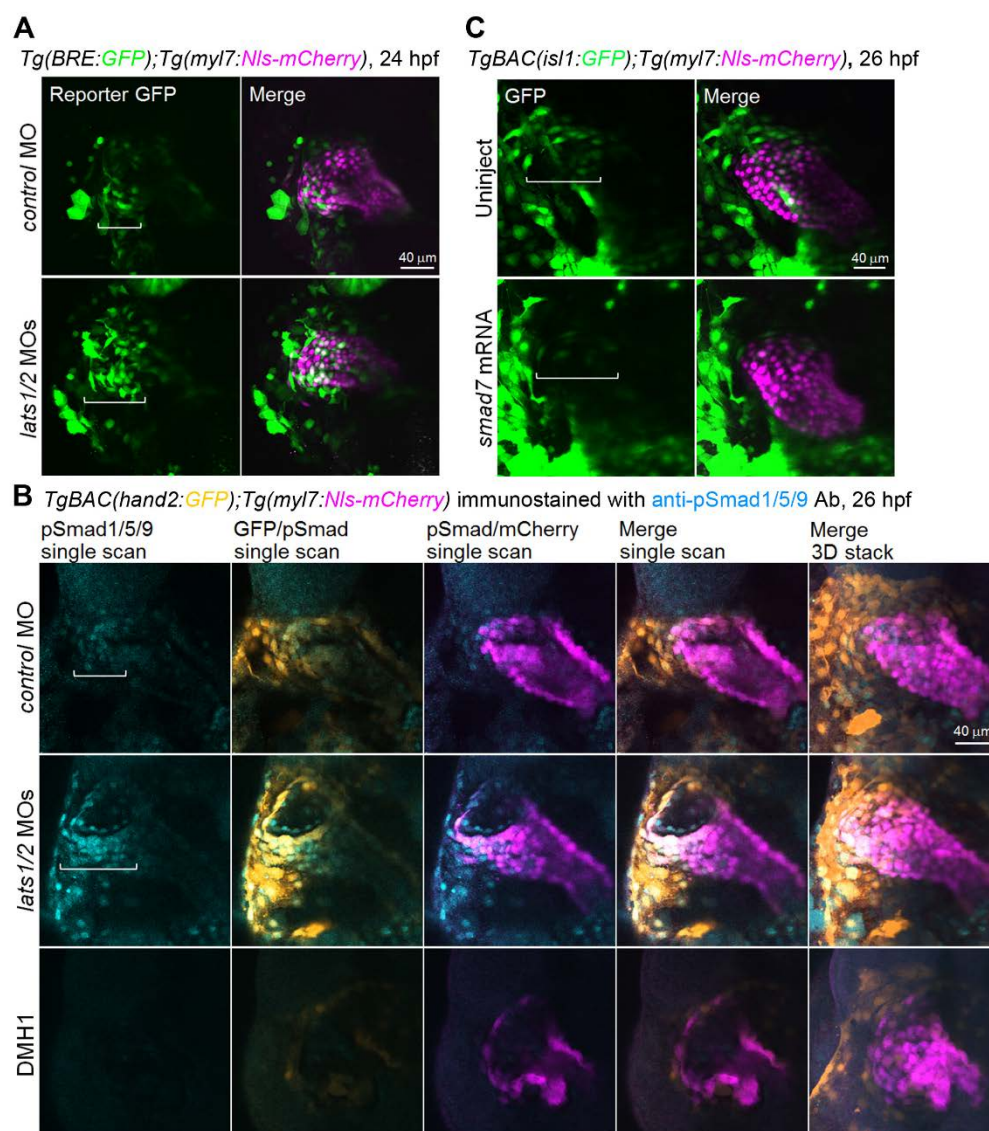30-05-2017-RA-eLife-29106

1169

**Figure 5—Figure supplement 1.** Depletion of Lats1/2 leads to an increase in the expression of *hand2*. **(A-C)** Whole mount in situ hybridization (WISH) analyses of the embryos of the control (uninject, left panels) and injected with *lats1/2* MOs (right panels) using antisense probe indicated at the left side of panels at the 10 somite stage (ss). **(A)** Brackets indicate the gap between *hand2*-positive regions of ALPM and PLPM. Note that the gap is absent in the *lats1/2* morphants. **(B)** Brackets indicate the *tal1*-positive rostral end of PLPM in the control. Note that the region indicated by the bracket in the uninjected embryo is absent in the *lats1/2* morphants. Dorsal view, anterior to the top. WISH images are a set of representative images of four independent experiments.
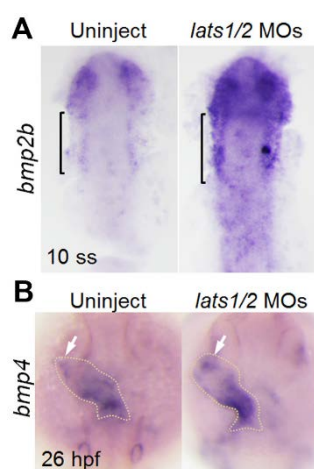
1179

1180

eLIFE -Research article (Full Submission)-
Fukui et al.
30-05-2017-RA-eLife-29106

1181

1182    **Figure 6—Figure supplement 1.** Depletion of Lats1/2 leads to an increase in the *bmps*

1183    expression. **(A, B)** WISH analyses of the embryos at 10 ss **(A)** and 26 hpf **(B)** of the control

1184    (uninject, left panels) and injected with *lats1/2* MOs (right panels) using antisense probe for

1185    *bmp2b* **(A)** and *bmp4* **(B)**. **(A)** Brackets indicate the *bmp2b*-positive left ALPM. **(B)** Arrows

1186    indicate the *bmp4*-positive cells in the venous pole. Broken lines indicate the heart tube. WISH

1187    images are a set of representative images of three independent experiments.

1188

1189

eLIFE -Research article (Full Submission)-
Fukui et al.
30-05-2017-RA-eLife-29106



**Figure 6—Figure supplement 2.** Depletion of Lats1/2 leads to an activation of Bmp-Smad signaling that is necessary for Isl1-positive SHF formation. **(A)** 3D confocal stack images of *Tg(BRE:GFP);Tg(myl7:Nls-mCherry)* embryos injected with the *control* MO and *lats1/2* MOs at 24 hpf. Brackets indicate the region of BRE-dependent GFP-positive *myl7* promoter-activated cells in the venous pole. **(B)** Confocal images of the *TgBAC(hand2:GFP);Tg(myl7:Nls-mCherry)* embryos injected with the *control* MO, *lats1/2* MOs, followed by the treatment with DMH1 (10 μM) from 14 hpf to 26 hpf (upper to bottom panels) and immunostained with anti-pSmad1/5/9 Ab at 26 hpf. Brackets indicate the phosphorylated Smad1/5/9-positive *myl7* promoter-activated cells in the venous pole. 3D confocal stack images (the most right panels) and single scan images (left four panels). Note that both *hand2* promoter-activated and pSmad1/5/9-positive cells in the venous pole are decreased in the embryos treated with DMH1. Dorsal view, anterior

59

eLIFE -Research article (Full Submission)-
Fukui et al.
30-05-2017-RA-eLife-29106

1202    to the top. **(C)** 3D confocal stack images of *TgBAC(isl1:GFP);Tg(myl7:Nls-mCherry)* embryos of

1203    the control (uninject, upper panels) and injected with 100 pg *smad7* mRNA (bottom panels) at

1204    26 hpf. Brackets indicate the region of *isl1* promoter-activated GFP-positive SHF cells in the

1205    venous pole. The confocal 3D-stack images and single-scan images are a set of representative

1206    images of at least three independent experiments.

1207

1208

eLIFE -Research article (Full Submission)-
Fukui et al.
30-05-2017-RA-eLife-29106

1209 **Legends for videos**

1210

1211 **Video 1.** *hand2* promoter-activated cells in the caudal region of the left ALPM move to venous

1212 pole. Time lapse recording of 3D-rendered confocal images of a *TgBAC*(*hand2:GFP*) embryo

1213 from 14 hpf (10 ss) to 26 hpf. Note the migration of caudal region of left (magenta) and right

1214 (cyan) ALPM cells toward venous pole and arterial pole of heart tube, respectively. Changes of

1215 colors reflect the tracking time (blue, 0 h; red, 12 h). Dorsal view, anterior to the top. The time

1216 lapse movie is a set of representative data of six independent experiments. Video 1 is related to

1217 Figure 3A, B.

1218

1219 **Video 2.** In the reversed-heart, *hand2* promoter-activated cells in the caudal region of the right

1220 ALPM move to venous pole. Time lapse recording of 3D-rendered confocal images of a

1221 *TgBAC*(*hand2:GFP*) embryo injected with *pkd2* MO from 14 hpf (10 ss) to 26 hpf. Note the

1222 migration of caudal region of left and right ALPM cells (magenta) was reversed. Changes of

1223 colors reflect the tracking time (blue, 0 h; red, 12 h). Dorsal view, anterior to the top. The time

1224 lapse movie is a set of representative data of four independent experiments. Video 2 is related

1225 to Figure 3A, B.

1226

1227 **Video 3.** Tead reporter-activated cells in the caudal region of the left ALPM move to venous

1228 pole. Time lapse recording of 3D-rendered confocal images of a *Tg(eef1a1l1:galdb-hTEAD2ΔN-*

1229 *2A-mCherry);Tg(uas:GFP)* embryo from 14 hpf (10 ss) to 24 hpf. Note the migration of Tead

1230 reporter-activated cells (magenta) in the caudal region of the left ALPM toward the venous pole

1231 of heart tube.    Changes of colors reflect the tracking time (blue, 0 h; red, 10 h). Dorsal view,

1232 anterior to the top. The time lapse movie is a set of representative data of six independent

1233 experiments. Video 3 is related to Figure 3D, E.

1234

1235 **Video 4.** Bmp-Smad signal-activated cells in the caudal region of the left ALPM move to venous

1236 pole. Time lapse recording of 3D-rendered confocal images of a *Tg(BRE:GFP);Tg(myl7:Nls-*

1237 *mCherry)* embryo from 14 hpf (10 ss) to 24 hpf. Note that Bmp-Smad signal is activated in the

1238 caudal region of the left ALPM (cyan) and that those cells move to venous pole of heart tube.

1239 Changes of colors reflect the tracking time (blue, 0 h; red, 10 h). Dorsal view, anterior to the top.

1240 The time lapse movie is a set of representative data of six independent experiments. Video 4 is

1241 related to Figure 6A.

1242

1243

1244